UNIVERSIDAD DE CHILE
FACULTAD DE CIENCIAS FÍSICAS Y MATEMÁTICAS
ESCUELA DE POSTGRADO

ATMOSPHERIC DYNAMIC RESPONSE BY OBLIQUITY FORCING

TESIS PARA OPTAR AL GRADO DE
DOCTORA EN CIENCIAS DE LA INGENIERÍA, MENCIÓN FLUIDODINÁMICA

PRISCILLA VIVIANA NOWAJEWSKI BARRA

PROFESOR GUÍA:
MAISA ROJAS CORRADI
PROFESOR GUÍA 2:
PATRICIO ROJO RÜBKE

MIEMBROS DE LA COMISIÓN:
RENÉ GARREAUD SALAZAR
FABRICE LAMBERT
LAURA PÉREZ MUÑOZ

Este trabajo ha sido parcialmente financiado por *CONICYT* grant no. 21110653, *FONDECYT* project no. 1171773, *NC120066*, and *FONDAP* no. 15110009.

SANTIAGO DE CHILE
AGOSTO 2019

RESUMEN DE LA TESIS PARA OPTAR AL
TÍTULO DE DOCTORA EN CIENCIAS DE LA INGENIERÍA, MENCIÓN FLUIDODINÁMICA
POR: PRISCILLA VIVIANA NOWAJEWSKI BARRA
FECHA: AGOSTO 2019
PROF. GUÍA: MAISA ROJAS CORRADI PATRICIO ROJO RÜBKE

ATMOSPHERIC DYNAMIC RESPONSE BY OBLIQUITY FORCING

En esta tesis presento la evolución de las variables atmosféricas que determinan el clima planetario al variar el parámetro de oblicuidad. Usando un modelo de circulación general de la atmósfera acoplado a un océano soméro con corrección de flujo por capa de mezcla, simulo 16 planetas de agua aumentando su oblicuidad entre 30° y 90°, los cuales presentan agua líquida en su superficie, permitiendo la aparición de formación de hielo marino como consecuencia de su dinámica atmosférica.

La insolación es mantenida como constante en cada experimento, sin embargo cambiar la oblicuidad afecta la distribución de energia, el balance radiativo, y por lo tanto a la circulación de gran escala. Se observa una dinámica atmosférica similar a la terrestre en los planetas de agua con oblicuidad menor a 54°. Sobre este valor el gradiente de temperatura latitudinal se invierte provocando un nuevo régimen de vientos, afectando a la forma de las celdas de Hadley y Ferrel, además de cambiar la posición de la Zona de Convergencia InterTropical.

Como la húmedad y la temperatura determinan la habitabilidad terrestre, se presentan los valores de temperatura de bulbo húmedo como indice atmosférico de habitabilidad para planetas de agua tipo Tierra con temperaturas sobre la congelación. Los planetas de agua son habitables durante todo el año, en todas las latitudes para oblicuidades bajo 54°, sobre este valor la habitabilidad disminuye hacia los polos debido a las altas temperaturas.

This thesis present the evolution of the atmospheric variables that affect planetary climate by increasing the obliquity, using a general circulation model (PlaSim) coupled to a slab ocean with mixed layer flux correction.

The obliquity is increased between 30° *and* 90° *in 16 aquaplanets with liquid sea surface and perform the simulation allowing the sea ice cover formation to be a consequence of its atmospheric dynamics.*

Insolation is maintained constant in each experiment, but changing the obliquity affects the radiation budget and the large scale circulation. Earth-like atmospheric dynamics is observed for planets with obliquity under 54°*. Above this value, the latitudinal temperature gradient is reversed giving place to a new regime of jet streams, affecting the shape of Hadley and Ferrel cells and changing the position of the InterTropical Convergence Zone.*

As humidity and high temperatures determine Earth's habitability, the wet bulb temperature is introduced as an atmospheric index of habitability for Earth-like aquaplanets with above freezing temperatures. The aquaplanets are habitable all year round at all latitudes for values under 54°*; above this value habitability decreases toward the poles due to high temperatures.*

Para mi Chepita.

Agradecimientos

Esta tesis, que tiene una mezcla entre Física, Astronomía y Meteorología, no hubiese sido posible sin la ayuda de Maisa Rojas y Patricio Rojo, mis profesores guías, a quienes agradezco infinitamente por haberme dado la oportunidad de desarrollar el tema que me ha apasionado durante toda la vida. Quiero agradecer también a los miembros de mi comisión, René Garreaud, Laura Pérez y Fabrice Lambert, por ayudarme a mejorar mi tesis con sus comentarios, para que pudiera llegar a personas que estén interesadas en el tema o que lo estuvieran desarrollando.

Quiero aprovechar esta instancia para agradecer a toda la gente que estuvo involucrada, de alguna u otra forma, en todo mi proceso estudiantil.
Quiero agradecer a mis profesoras de ciencias naturales del colegio, ya que ellas fueron parte de los modelos a seguir que tuve desde pequeña. Gracias a ellas jamás pensé que ser mujer sería un impedimento para estudiar ciencias.

A mis profesores Mónica Rubio, Luis Barrera y Gonzalo Palma, muchas gracias por haber creído en mí, dándome la oportunidad, el apoyo y los espacios para desarrollarme como investigadora. A José Rutllant y Humberto Fuenzalida por transmitirme todo su amor por la meteorología y la historia, les agradezco por haberme dado la confianza de poder entrar a sus oficinas cuando yo quisiera solo para conversar, fuera en el DGF o en la DMC. Son horas invaluables de mucha amistad y conocimiento que siempre voy a recordar con mucho cariño.

Quiero agradecer a mis amigos y amigas que siempre estuvieron apoyandome en distintas etapas del doctorado. Lo más probable es que esta tesis hubiese costado mucho más sin su ayuda.
A Ismael Botti, por todas esas grandes aventuras que pasamos con Roberto Troncoso que todavía me sacan risas al recordarlas. Por todos los años de estudio en la Biblioteca de Providencia y el Café Literario donde vivíamos a café, matemáticas y copuchas haciendo tareas interminables, que al final se convirtieron en horas de compañía escribiendo nuestras tesis de doctorado.

Mis compañeras y compañeros de oficina y postgrado, Jorge Jara, Cecilia Farías, Pamela Pizarro, Sergio González, Cristian Muñoz y Alejandra Molina, Valeria Rudloff y Mónica Bello, gracias a todos Uds. por apañar con buena onda en todas esas horas de trabajo que no terminaban nunca, con harto tecito cuando había que esperar esas corridas en el computador que nos hacían pasar rabia. Gracias por todos los retos chasconeados y todos los momentos compartidos en esas horas interminables de universidad, cuando nos quedábamos trabajando en la noche y siempre éramos los últimos en irnos. También a mis amigos y amigas, Laura

Flores, Danitza Villouta, Alejandro Roldán, Luz María Fariña, Sebastián Carrasco, Stefano Cararo y Sebastián Obando, a todos Uds., muchas gracias por permitirme ser parte de sus vidas y por todos los consejos, pero sobre todo gracias por escuchar mis ideas locas sobre vida y planetas, por aceptar mis ideas revolucionarias, por aceptar mi imposibilidad de llevar conversaciones largas sin distraerme y también, porque juntos rompimos el estándar de que meteorólogos y sismólogos no se llevaban bien.

Sin embargo, el agradecimiento más importante va a mi familia, quienes están ahí en mi día a dia, en mis alegrias y mis frustraciones.
A mi Alexander, un hombre tan increíble como el increíble lugar donde lo conocí, tan sacado como de otro planeta que hasta el Pepi lo sabe. Hemos pasado por tantas cosas en tan poco tiempo y me has apoyado en todo, sin cortarme las alas con ideas convencionales, siempre apoyándome, hasta en mis ideas más increíbles y, sobre todo, aterrizándome. Eres mi consejero frente a los impulsos, los que he aprendido a analizar desde otra perspectiva gracias a ti. Te tocaron los años más duros de mi doctorado y por fin toda mi impaciencia está llegando a su fin (en teoría). Ahora, el cielo es el límite y hay que aprovechar el impulso porque sé que siempre vamos a ir por más, somos el tremendo equipo!

A la Mona, la Isa y mi Chepita por darme el apoyo de seguir una carrera no convencional, aunque muchas veces no entendieron porque no trabajaba en una oficina. A ti mamita, te dedico esta tesis, porque eres la que siempre ha creído en mi incluso cuando el mundo se ha puesto en mi contra, por qué siempre has estado convencida de que ser científica es lo mejor del mundo y por ser la mujer más importante de mi vida, la que me ha enseñado lo que es el sacrificio y la perseverancia, porque con esfuerzo se consiguen las cosas y a ser siempre la más ruda cuando hay que serlo, pero siendo humilde y siempre ayudando a los que lo necesitan. Y mis perritos! Mi Pepito y Panchito que siempre han estado ahí acompañandome en las largas horas y años de estudio, con el amor más incondicional y agradecido que he conocido en la vida. A todos los demás que han ido llegando y a los otros que se han ido, porque parece que se van pasando el dato de que en nuestra casa los recibimos a todos.

Estoy segura que se me queda mucha gente en el tintero, pero quiero agradecerles a todos a quienes he conocido, ya que sin Uds., no sería la persona que soy ahora y nada de esto hubiese pasado. A todos quienes están leyendo...Muchas Gracias.

Contents

Chapter 1

Motivation

In 1995 the first planets were discovered outside our solar system (Mayor and Queloz, 1995). This discovery motivated the scientific community to discuss the existence of life outside Earth and what would be the conditions for its proliferation.

The existence of liquid water determines planetary habitability. Necessary for metabolic processes in different species, water is the primary target for current space missions (Catling, 2013). Several factors settle the existence of liquid water on a planet. The first condition is the planet-star distance since it determines the amount of radiation the planet receives and therefore defines the Habitable Zone (Kopparapu et al., 2013), the region where the chances of finding liquid water on the surface of the planet increase. This Habitable Zone is also the region where space missions focus their search.

However, Lammer et al. (2010) shows the importance of the planet's geophysics in habitability studies. Maintaining global temperatures above the freezing point depends not only on the distance to the star but also on the internal processes of the planet. The atmosphere plays an essential role as its components interact with solar radiation producing a greenhouse effect which sustains a warm global climate, in addition to the existence of a differential heating created by the absorption of solar radiation which promotes the circulation of air masses between latitudes.

Showman et al. (2010) indicates that although the general circulation of Earth's atmosphere is known and used to understand the atmospheric behavior of other planets. The atmospheric circulation depends on various factors such as the stellar flux and the planet's orbital parameters, rotation rate, mass, atmospheric chemical composition, and surface composition. Therefore, the discovery of extrasolar planets with diverse characteristics means a big challenge for the atmospheric sciences, especially for the development of atmospheric models. These new worlds have added a more significant range of parameters that affect the theory of the general atmospheric circulation, so that a terrestrial model fails to adequately characterize another planet, leaving in evidence the need to find a unified theory for all cases.

Seager (2013) indicates the importance of the orbital parameters for the study of planetary habitability. The obliquity is used in this thesis, because it is the orbital parameter that determines the latitudinal distribution of incoming stellar radiation (insolation) at the top of the planet's atmosphere, causing the occurrence of seasons and affecting the development of the general atmospheric circulation.

The approach of this thesis is comparable with the works of Linsenmeier et al. (2015), Ferreira et al. (2014), Williams and Pollard (2003). They present the effects of changing the obliquity on the atmospheric dynamics of Earth-like aquaplanets, indicating that the occurrence of liquid water is a consequence of the atmospheric activity, determined by the change in the latitudinal distribution of insolation, on which the surface temperatures depend. Linsenmeier et al. (2015) focuses its study on climatic multistability, showing the necessary conditions for the coexistence of ice-free and ice-covered regions. Their habitability parameter is the sea ice cover which develops on the surface as a consequence of the atmospheric activity. On the other hand, Ferreira et al. (2014) shows the role of the ocean by increasing the obliquity focused mainly on the study of surface wind patterns and the ocean ability to modulate extreme temperature values produced between hemispheres. Finally, Williams and Pollard (2003) studies the climate evolution of Earth-like planets by varying the continental distribution and greenhouse gases concentration relative to current Earth's configuration. The study searches the conditions that could trigger a runaway greenhouse effect or global freezing in these type of planets.

Most obliquity studies have not used more than three extreme values, usually 0°,54° and 90° whose effects are compared with the current obliquity value of Earth, 23.5°. The exception is given by Williams and Pollard (2003) that uses 12 values of obliquity between 0° and 85° with different continental configuration. This thesis presents the simulation of 16 aquaplanets with obliquities between 30° and 90° where the existence of liquid water on its surface is ensured. Obliquity values less than 30° have been left out from this thesis as they present latitudinal surface temperatures where sea ice formation is possible. It is not part of the scope of this thesis to study habitability in the multistability climate regime, where warm conditions and sea ice cover coexist (Lucarini et al., 2013).

The obliquity of 54° is included as the value where the latitudinal distribution of insolation is reversed, becoming higher in the poles than in the equator (Ward, 1974). Although this effect is well documented in the works of Ferreira et al. (2014), Williams and Pollard (2003), Linsenmeier et al. (2015) indicates that this transition occurs at the obliquity of 55°. For this inconsistency concerning previous research, in this thesis, a finer grid of obliquities is presented, centered around 55°, including also 54° of obliquity, to identify any phenomenon that could be associated with the model configuration.

As in Linsenmeier et al. (2015), the simulations of this thesis were performed with Planet Simulator (PlaSim), a general atmospheric circulation model coupled to a slab ocean of 50 m depth, without ocean currents. Using this depth value produces a similar response to real ocean according to Donohoe et al. (2014). Moreover, the simulations include a mix layer flux correction that simulates the oceanic heat flux. Thus, this is an intermediate configuration between the one used by Linsenmeier et al. (2015), who do not use flux correction and the full coupled model of Ferreira et al. (2014), which includes ocean currents interaction.

Aquaplanets have been widely used to understand Earth's climate, e.g., Marshall et al. (2007), Enderton and Marshall (2009), Williamson et al. (2013). Aquaplanets are simplified experiments used to explore the climate responses ignoring zonal asymmetries introduced by continents (Williamson et al., 2013), the main reason to use this type of configuration in obliquity studies (Linsenmeier et al., 2015, Kilic et al., 2017).
Most of these studies were carried out with atmospheric models and a slab ocean, therefore focusing on the role of the atmosphere in the heat transport. Ferreira et al. (2014) using a fully coupled Atmosphere-Ocean General Circulation Model (A-OGCM) in aquaplanet mode found that the ocean of an aquaplanet with 90° of obliquity turns into a heat reservoir, maintaining warm temperatures even at the hemisphere that is in complete darkness, similar to slab ocean results. The next paragraphs present the objectives of this thesis.

This thesis will present the effect on the atmospheric dynamics and habitability of Earth-like aquaplanets by changing its obliquity. The main focus is to explore the conditions that produce the atmospheric circulation and its consequences due to the strong dependence on obliquity change. In particular, this thesis will present how the changes in atmospheric circulation influence the planetary habitability as an atmospheric parameter.

Unlike previous obliquity research, this thesis presents 16 simulations with obliquity values between 30° and 90°, which ensure a warm climate. When freezing occurs, it is solely due to the atmospheric activity of the planet. It is not part of the objectives of this thesis to introduce changes in the continental configuration, nor atmospheric chemical composition.

On the other hand, these 16 simulations allow deriving with higher precision the changes in the atmospheric variables of importance for planetary habitability, as well as to establish empirical equations for the global surface temperature and to observe the evolution of the variables that determine the heat distribution in the atmosphere. Thus, it will be possible to verify that the reversal of the temperature gradients is only related to the increase in obliquity. It will allow to identifying the obliquity value where the zonal jet begins its development as described by Linsenmeier et al. (2015), Ferreira et al. (2014), or to observe the changes described by Williams and Pollard (2003) in the Intertropical Convergence Zone due to the decrease in Hadley cells height since, by producing less mass movement from the surface, precipitation decreases.

Finally, in this thesis, the habitability study is performed on Earth-like aquaplanets that fulfill the condition of exhibiting liquid water on its surface, but unlike previous works that study habitability according to the ice coverage on its surface, in this case, the habitability of these aquaplanets will be limited by their high temperatures. Thus, the wet bulb temperature is presented as an index of atmospheric habitability by associating relative humidity and air temperature to establish an upper limit of habitability for mammals at $35°C$.

This thesis is organized as follows: Chapter 2 presents the fundamental concepts necessary to understand the general atmospheric circulation. Chapter 3 shows the methodology, including the parameters defined to perform the simulations, in addition to the data processing and the description of the model used. Chapters 4 and 5 present the results and conclusions already published (Nowajewski et al., 2018).

Chapter 2

Basic Concepts

This chapter presents the notions mentioned in the introduction, as the concept of planetary habitability, the importance of the orbital forcing, and the general circulation of the Earth's atmosphere.

2.1 Planetary habitability

More than 30 years ago, the existence of life outside the Earth was considered a philosophical question, despite this, Carl Sagan was the pioneer in encouraging the search for extraterrestrial life, managing to persuade institutions like NASA to send terrestrial messages in the space missions as Pioneer, thinking about the possibility of making contact with other civilizations. Moreover, Frank Drake proposed the estimation of the number of intelligent civilizations that could exist in the universe, also seeking to stimulate scientific discussion on the subject. It was not until 1995 when these assumptions received scientific evidence as Mayor and Queloz (1995) discovered the first planet outside of our Solar System.

The development of space mission technology allowed the number of extrasolar planets to increase exponentially. The implementation of the Kepler mission in 2009, accomplished the discovery of thousands of new extrasolar planets outside our Solar System, identifying planets with different sizes, some of them as smaller as our Earth, in the vicinity of Sun-like stars. Today we know that statistically, there is at least one planet for each star in the universe (Borucki et al., 2008, 2011, Batalha et al., 2013). In this scenario, the expected question is, Could it be that one of these planets can harbor life? The essential element for life to exist on our planet is water. For this reason, the search for life on other planets focuses on planets that may have liquid water on its surface and even below its surface, as it is the case of some celestial bodies of the Solar System. Therefore, planetary habitability is defined as the capacity of a planet to sustain liquid water on its surface, maintaining and supporting the proliferation of life (Catling, 2013).

Shapley (1953) referred to the existence of a liquid water belt around the stars. Currently, this region is known as the Habitable Zone (HZ). In this area, a planet has the highest probability of maintaining liquid water on its surface. The location of HZ depends mainly on stellar type as the region is determined by the temperature of the star (Kopparapu et al., 2013).

The HZ extension has been estimated for different types of stars, depending on the stellar properties and the response of the planet's atmosphere to the stellar flux forcing (De Vera et al., 2013). The inner edge of HZ is defined as the closest location to the star. Because of this proximity, the planet can experience a strong runaway greenhouse effect, losing its atmosphere by evaporation. On the other side, the outer edge is far from the star. By convention, at this edge, the condensation of carbon dioxide by low temperatures occurs (Catling, 2013)

Venus, the Earth, and Mars are located within the Sun's HZ. Kasting (1988) indicates, Venus, located in the inner limit of HZ, experienced the evaporation of the water present in its early stage. Due to its proximity to the Sun (0.7 AU), the high temperatures increased the hydrogen escape rate into space, leaving a high concentration of CO_2 in its atmosphere, causing the greenhouse effect that we see today. Located at the outer limit of HZ, Mars with its thin atmosphere maintained by its low gravity, failed to warm the surfaces by the greenhouse effect. Its global temperatures reach up to $-60°C$, exhibiting the condensation of carbon dioxide in its surface. The Earth is located in the middle of Sun's HZ, allowing water to remain liquid at its surface. According to Hart (1978), the Earth could either experience runaway greenhouse effect or quickly fall into a snowball state, if this equilibrium position changed a small percentage. Currently, the Sun's HZ area extends between 0.95 AU and 1.67 AU (Kopparapu et al., 2013). However, this range can vary depending on the behavior of the planet's atmosphere, since the presence of clouds could decrease the inner range of HZ, by reflecting the incoming radiation and hence cooling the surface of the planet. Figure 2.1 shows the position and extension of HZ for different stellar types.

For a planet to be habitable, the surface temperature must be mild enough to avoid runaway greenhouse effect or snowball state (Kasting, 1988, Sugiyama et al., 2005, Spiegel et al., 2008). Besides the external forcing, several processes related to the planet geophysics also determine the existence of liquid water on the planet's surface. Both Williams and Kasting (1997), Dressing et al. (2010) indicate an ocean-land configuration give a stable climate even when large fluctuations of its orbital parameters occurs. In particular, Williams and Pollard (2003) shows Earth-like planets with different continental distribution maintain their temperature without falling into a runaway greenhouse effect nor snowball state by changing its obliquity. Moreover, Linsenmeier et al. (2015) indicates planetary habitability depends on the ice cover, as snowball state planets are usually discarded as habitable. Hence, to understand the conditions for a planet to be habitable, it is necessary to understand the problems related to its climate system and the response to external forcing. The current theory of atmospheric circulation applied to extrasolar planets was initially developed for the Earth and depends on the atmospheric mass, composition, stellar flux, rotation rate, and orbital parameters. With the investigation of the atmosphere of the extrasolar planets, we can expand the range of parameters that can affect the dynamics of the atmosphere, broadening the understanding of atmospheric circulation theory Showman et al. (2010).

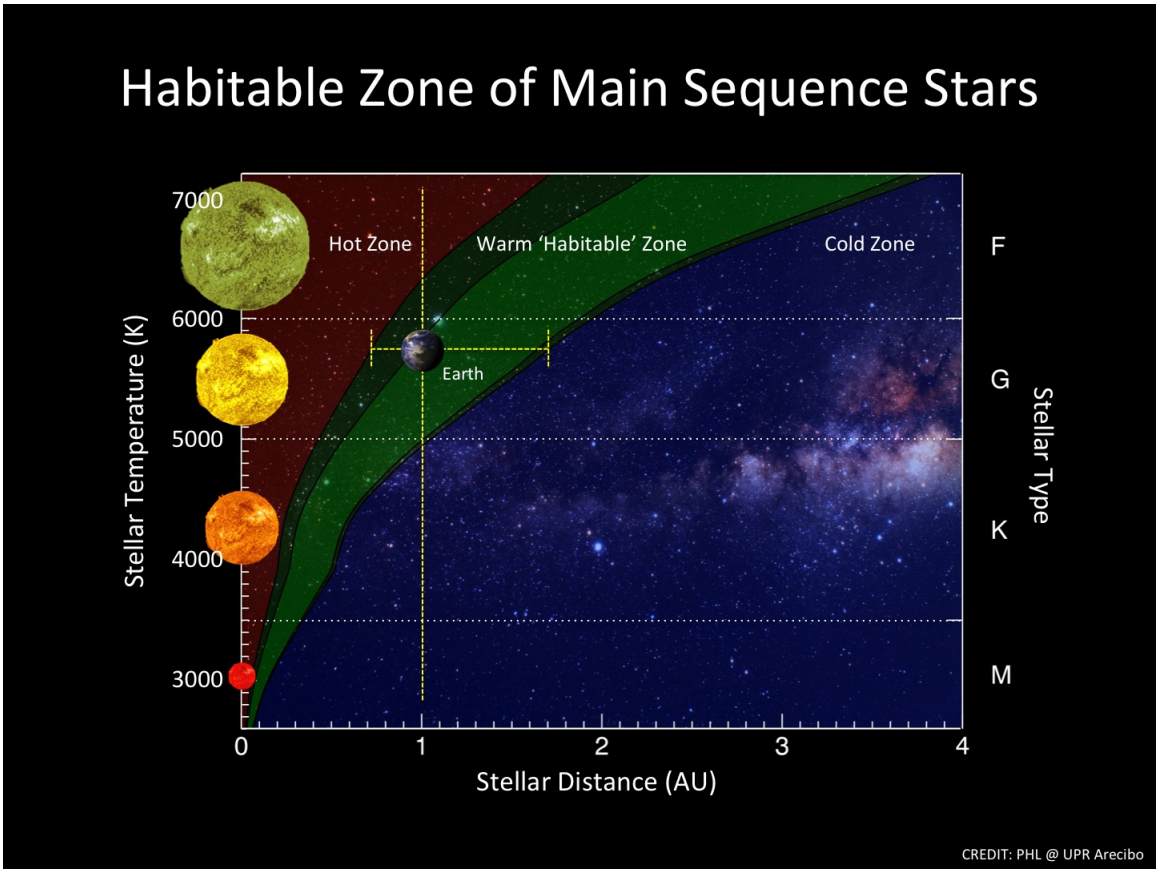

Figure 2.1: The figure shows the position of HZ depending on the star type. The Green area shows the HZ or the region surrounding a star with a high probability of finding liquid water on the surface of a planet. The location of HZ moves away from the star as the temperature increases. The dark green area shows the "Optimistic Habitable Zone" where the inner extension of HZ expands depending on the planet's atmospheric variables such as cloud cover. The red area shows the inner region of HZ where the runaway greenhouse effect occurs due to the proximity to the star. The blue area shows the outer edge of HZ where the planet falls into a snowball state. From PHL UPR Arecibo.

2.2 Orbital forcing

Obliquity δ, eccentricity ε and precession Λ are the main orbital parameters that affect a planet's climate. These parameters affect the amount of incident flux at the top of the atmosphere (Cowan et al., 2012) by changing the latitudinal distribution and seasonal pattern of the insolation (Berger, 1988).

The focus of this thesis is to use obliquity as the forcing factor that will determine the climate system of the simulated planets. The obliquity is the angle between the planet's spin axis and the normal to its orbital plane, producing an inclination that distributes the incident radiation latitudinally (see Figure 2.2). This inclination causes the increase of energy received by the latitudes that face the star (Berger, 2012).

A consequence of the planet obliquity is the existence of seasons, e.g., if a planet has $\delta = 0°$, this planet does not present seasons since the incident radiation is constant throughout the year for each latitude. Meanwhile, a planet with $\delta = 90°$ presents extreme seasons at high latitudes. Current Earth's obliquity[1] is 23.44°, meaning higher insolation at the Equator than Poles. This differential heating between high and low latitudes influences the distribution of the energy flux in the planet.

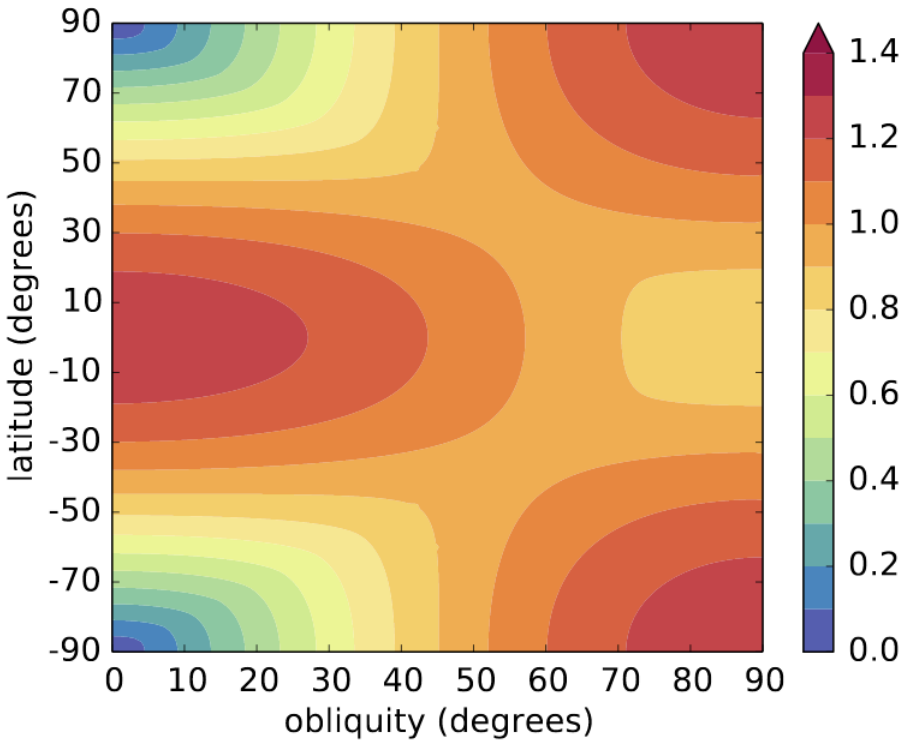

Figure 2.2: Transition of the annual mean latitudinal distribution of insolation by changing the obliquity in a planet with a circular orbit $\varepsilon = 0$. Colorbar indicates the global mean insolation as a fraction of $S/4$ where S is the solar constant. As the obliquity increases, Poles receives more insolation than the Equator. From Linsenmeier et al., arXiv:1401.5323v4, 2014. With permission

Earth's obliquity is not a fixed value; in fact, has a cycle of 41,000 years with values varying around 22° and 25° as indicated by Crucifix et al. (2006). Imbrie et al. (1993) indicated this 2° of variation in δ considered as highly stable, but enough to be responsible for the glacial-interglacial cycles, prevalent in Earth's climate over the last two million years approximately stated by Milankovitch's theory.

According to Laskar et al. (1993), the tidal effect of the Moon stabilized Earth's obliquity. This stability results in small latitudinal variations in the distribution of the incoming radiation at the top of the atmosphere, keeping a stable climate, essential for the proliferation of life. Without the Moon, Earth would enter into a chaotic window with obliquity values fluctuating between 60° and 90°.

[1] https://nssdc.gsfc.nasa.gov/planetary/factsheet/earthfact.html

Laskar and Robutel (1993) determined that δ can be affected by gravitational disturbances caused by the presence of other planets and internal forces acting on the planet. For this reason, a planet with an initial 0° obliquity ends with a chaotic obliquity, e.g., Mars is currently in the chaotic window. Touma and Wisdom (1993), Bills (1990) indicates the variation of Mars's obliquity between 0° and 60° over a 100,000 years cycle. However, in the Solar system, most of the planets have a stable obliquity. Mercury and Venus have managed to stabilize their obliquity by tidal forces effect, and giant planets maintain their obliquity stable since the final phase of the Solar System's formation.

Bodies with high obliquity are not a rarity in our solar system. Venus has an obliquity of 0° with retrograde rotation. Neptune and Uranus have inclinations of 30° and $\approx$ 90° respectively, whereas Pluto has an obliquity of 54° with retrograde rotation (Dobrovolskis and Harris, 1983). As mentioned, 54° of obliquity has a special geometrical meaning since the planet receives the same insolation over a year at the equator and the poles.

2.2.1 Radiation

The quasi-equilibrium state observed in Earth's atmosphere depends on the balance between the amount of incident solar radiation and the thermal radiation emitted by the planet (Abbot, 1917). Since solar radiation enters at the top of the atmosphere, it is absorbed, scattered and reflected by the atmospheric compounds in its journey to the surface. Only a percentage of the incident solar radiation reaches the planet's surface. Figure (2.3) shows the annual mean global energy budget as a diagram of the interactions between solar radiation and the Earth's climate system. According to (Trenberth et al., 2009), on the atmosphere, solar radiation interacts with atmospheric gases and clouds. The gases are responsible for absorbing and scatter solar radiation in every direction. The absorbed fraction is added to the planet's heat budget, while a fraction of the scattered radiation returns to space. The presence of clouds plays an essential role in the radiative balance by affecting the reflectivity, the absorptivity, and transmissivity of incident solar radiation.

After crossing the atmosphere, solar radiation is absorbed and reflected by the surface. The amount of absorbed radiation will depend on the presence of oceans, soil, snow or ice, as they vary the reflectivity of the surface, hence changing its albedo (Robock, 1980). The albedo (A) is the ratio between the reflected solar radiation and the incoming solar radiation. At lower reflectivity, higher is the absorbed radiation, e.g., in the surface, liquid water is capable of absorbing more incident solar radiation than soil. The incident solar radiation, continuously absorbed by the atmosphere and the surface, return to space as thermal radiation or long-wave radiation, which is emitted by the heating of the components of the planet's climate system. Before leaving the planet, the emitted thermal radiation is also absorbed and scattered by the atmosphere and reflected toward the surface. On Earth, carbon dioxide, and water vapor absorb the thermal radiation, while clouds reflect a percentage of this radiation toward the surface.

According to Peixoto and Oort (1992), the net radiation flow at the surface F_{rad}^{sfc}, responsible for its heating, will be given by the difference of incoming solar radiation plus the absorbed thermal radiation and solar radiation transmitted and reflected plus the outgoing

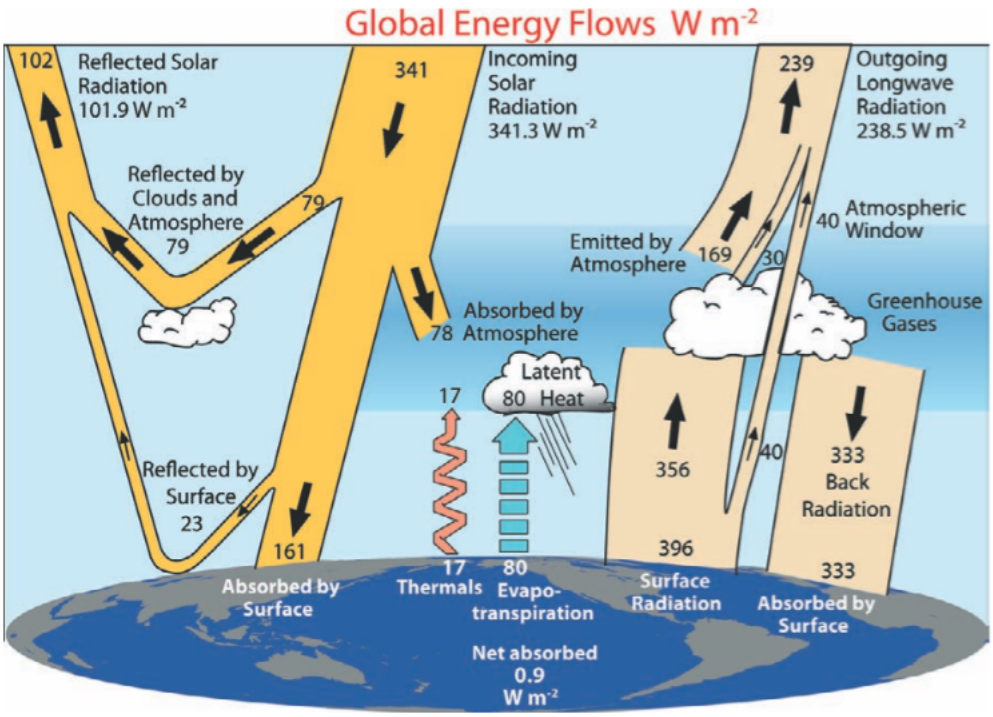

Figure 2.3: Earth's energy budget diagram. From 100% incoming solar radiation that enters at the top of Earth's atmosphere, about 70% interacts with the components of the climate system while the remaining 30% is reflected to space. Some regions absorb more radiation than others, creating a differential heating in the surface, producing the emission of thermal radiation. This radiation goes out into space after interacting with the components that produce the greenhouse effect in the atmosphere which retains 95% of the thermal emission, warming the surface. (From Trenberth et al., Bulletin of the American Meteorological Society, vol. 90, no 3, p. 311-323. 2009. With permission.)

thermal radiation. The radiation budget equation is:

$$F_{\text{rad}}^{sfc} = F_{SW}^{\downarrow}\,(1 - A) - \varepsilon\,\sigma\,T_{sfc}^{4} + F_{LW}^{\downarrow}$$

Where A is the albedo at the surface, ε is the emissivity of the atmosphere, σ is Stefan-Boltzmann constant, T_{sfc} is surface temperature and $F_{LW}^{\downarrow}$ is the incident thermal radiation that comes from the atmosphere.

Finally, at the top of the atmosphere, the amount of solar (short-wave) radiation absorbed is compensated by the same amount of thermal (long-wave) radiation emitted by the planet into space, allowing the climate system to be in radiative equilibrium $F_{rad} = 0\ Wm^{-2}$. Without this balance, the planet will run under global radiative heating or cooling.
Kiehl and Trenberth (1997) indicates how radiative processes act cooling high latitudes and warming low latitudes on Earth. Figure (2.4) shows the Earth's latitudinal radiation balance in the annual mean where a surplus of absorbed solar radiation is observed at low latitudes, while a deficit occurs at high latitudes.

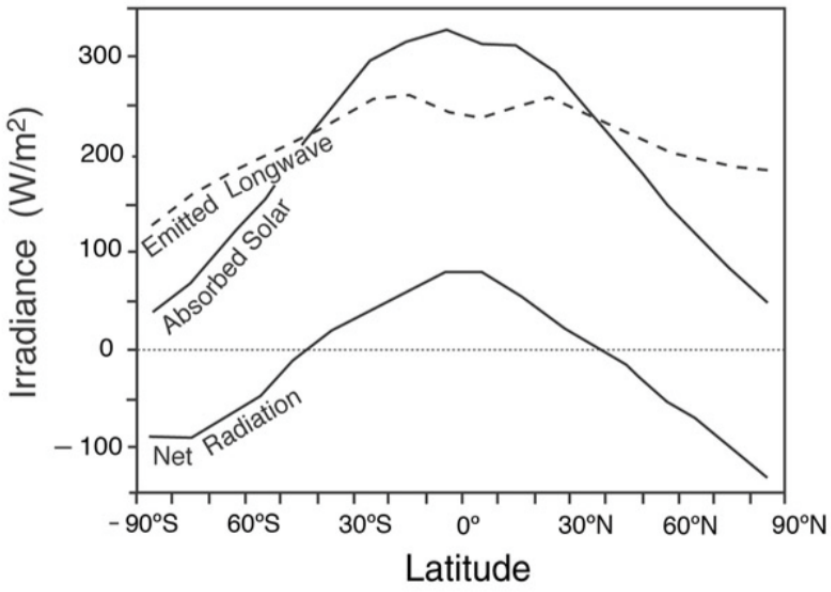

Figure 2.4: Net radiative budget. Earth's annual mean absorbed solar radiation, emitted long-wave radiation and net radiation (Wm^{-2}) at the top of the atmosphere. Poles present a deficit of absorbed radiation due to a greater emission of long-wave radiation into space, shown as negative values in the net radiation curve. Further, a surplus of absorbed radiation occurs at the equator where less long-wave radiation is emitted to space (positive values in net radiation curve). (From Marshall et al., Academic Press, 2016. With permission)

2.2.2 Temperature

The planet's global temperature will depend on the atmospheric compounds and the reflectivity of the surface. These variables determine the amount of solar radiation absorbed, and the amount of thermal radiation emitted (Ingersoll, 2013).

The surface temperature of a planet with a thin or negligible atmosphere corresponds to its equilibrium temperature determined by the albedo and the energy flow from the star. The Equilibrium Temperature corresponds to the black body temperature described by the Stefan-Boltzmann law:

$$T_{\mathrm{e}} = \left[\frac{(1-A)F_0}{4\sigma}\right]^{\frac{1}{4}}$$

Where A is the planet's albedo, F_0 is the energy flux from the star and $\sigma = 5.67 \times 10^{-8} W\, m^{-2}\, K^{-4}$ is the Stefan-Boltzmann's constant.

Sanchez-Lavega (2011) indicates the surface temperature on a planet with a dense atmosphere increase by the interaction between the semi-opaque atmospheric components and the thermal radiation emitted by the planet. These components generate a greenhouse effect since they allow only a part of this thermal radiation to be released into space, while the other part is reflected toward the surface and absorbed by it, increasing its temperature.

On Earth, greenhouse gases such as water vapor and CO_2 absorb this thermal radiation, while clouds and some aerosols reflect the radiation towards the surface. The surface temperature can be written in terms of the equilibrium temperature and the greenhouse effect as:

$$T_{sfc} = T_{\mathrm{e}} + \Delta T$$

Where ΔT corresponds to the temperature increase on the surface due to the presence of atmopsheric greenhouse gases. According to (Lindzen, 1994), the temperature difference that exists due to the greenhouse effect on Earth is $\Delta T = 33\,K$, with $T_{\mathrm{e}} = 255\,K$ and $T_{sfc} = 288\,K$.

The latitudinal distribution of insolation determined by the obliquity of the planet will produce regions with surplus and deficit of absorbed radiation, causing a differential heating in the planet. Peixoto and Oort (1992), indicates on Earth with an obliquity of 23.5°, the highest temperature occurs in the Equatorial region, with temperatures that show low fluctuation throughout the year. While the polar regions have the lowest temperature on the planet, with high fluctuation of temperatures during the year, since the incident solar radiation reaches $0\,Wm^{-2}$ in winter. Figure (2.5) shows the annual mean temperature on Earth, both in its latitudinal distribution and in its vertical extension. The chemical composition of the atmosphere determines the vertical distribution of temperatures. Temperatures decrease with height in the troposphere and increase in the stratosphere, due to the presence of atmospheric ozone which absorbs solar radiation, increasing the temperature of the layer. The temperature gradients observed are the main source of energy available for the movements that characterize the atmospheric circulation.

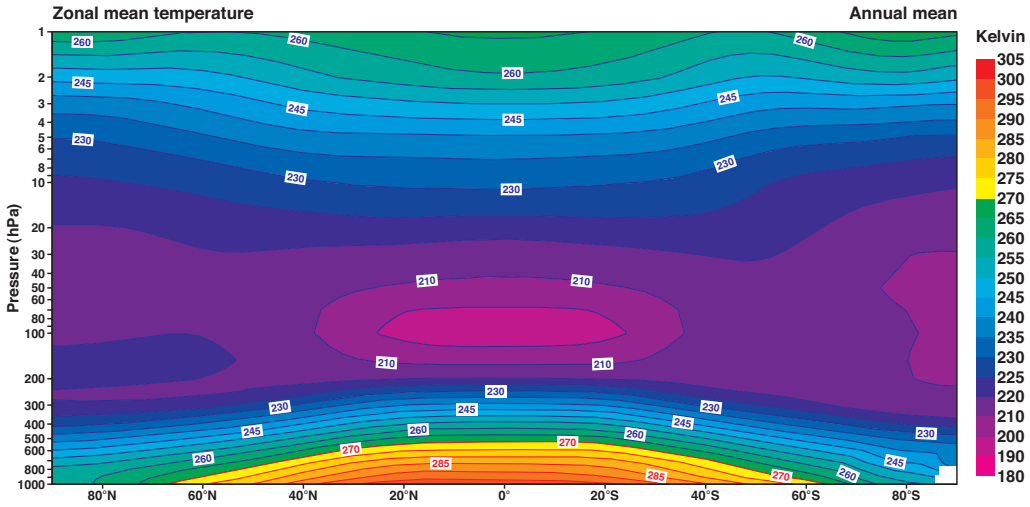

Figure 2.5: Vertical profile of Earth's temperature. From the South Pole to the Equator, the temperature increases homogeneously due to the larger portion of the ocean located in the Southern Hemisphere. The distribution of temperature in the Northern Hemisphere is affected by continents as its heat capacity is lower than the oceans. (Zonal mean temperature - stratospheric perspective using ERA-40 Atlas from Pressure level climatologies, ECMWF, Kallberg et al. (2004))

2.3 General circulation of the atmosphere

As (Showman et al., 2010) indicates, the general circulation of the atmosphere is a problem of coupled radiation and hydrodynamics. Although differential heating produces the circulation of the atmosphere, it is the existence of the atmosphere that allows the heating or cooling patterns to exist. The atmosphere is a spherical layer of fluid that surrounds a planet, maintained by its gravity, with the radiation from its host star as its primary source of energy. The spherical geometry of the planet results in incident solar radiation (normal to the surface) not being distributed homogeneously in high and low latitudes, creating a differential heating in both regions (Marshall and Plumb, 2016).

Earth's atmosphere is baroclinic; this means that its density depends on the pressure and temperature ($\rho = \rho(p, T)$). Thus, when there is surface differential heating between low and high latitudes, the pressure contours (isobars) are inclined vertically, causing baroclinic instability. This instability attempts to balance the potential energy of the isobar when it acquires an inclination due to a horizontal temperature gradient. Thus, by decreasing its height, the potential energy of the isobar is converted into kinetic energy, particularly in the form of solenoids that move from the lower temperature to the higher temperature zones. On Earth, this instability is manifested by large-scale and mesoscale movement, such as frontal systems. As indicated by Vallis (2017), this movement is known as the general circulation of the atmosphere, where the pressure gradient produces wind patterns that transport heat between both regions with different temperatures.

2.3.1 Winds

The differential heating of the planet changes the atmospheric pressure, producing a general circulation in the atmosphere due to horizontal advection of air masses between warm and cold regions. As the atmosphere behaves as a fluid, its motion can be described by the Navier-Stokes equations. Following Peixoto and Oort (1992), Holton and Hakim (2012), Sanchez-Lavega (2011), these equations written in spherical coordinates (λ,ϕ,z,t) are:

$$\frac{Du}{Dt} = \frac{\tan\,\phi}{R}\,uv - \frac{uw}{R} + 2\Omega v \sin\,\phi - 2\Omega w \cos\,\phi - \frac{1}{\rho R\cos\phi}\frac{\partial p}{\partial \lambda} + F_\lambda \tag{2.1}$$

$$\frac{Dv}{Dt} = -\frac{\tan\,\phi}{R}\,u^2 - \frac{vw}{R} - 2\Omega u \sin\phi - \frac{1}{\rho R}\frac{\partial p}{\partial \phi} + F_\phi \tag{2.2}$$

$$\frac{Dw}{Dt} = \frac{u^2+v^2}{R} + 2\Omega u\cos\phi - \frac{1}{\rho}\frac{\partial p}{\partial z} - g + F_z \tag{2.3}$$

Where

$$\frac{D}{Dt} = \frac{\partial}{\partial t} + u\,\frac{\partial}{\partial x} + v\,\frac{\partial}{\partial y} + w\,\frac{\partial}{\partial z}$$

Is the total derivative and λ is the longitude, ϕ is the latitude, ρ is the density, R is the radius of the planet, g the acceleration of gravity, p pressure and Ω is the angular velocity of the planet. (F_λ, F_ϕ, F_z) correspond to friction forces.

Moreover:

$$\begin{aligned} u &= R\cos\phi\frac{\mathrm{d}\lambda}{\mathrm{d}t} \\ v &= R\frac{\mathrm{d}\phi}{\mathrm{d}t} \\ w &= \frac{\mathrm{d}z}{\mathrm{d}t} \end{aligned}$$

Correspond to zonal wind components: zonal wind (u), meridional wind (v) and vertical wind(w). In the free atmosphere, the horizontal movements are intensified over $500\,hPa$, while the vertical movements are negligible by hydrostatic equilibrium (pressure balanced by gravity):

$$\frac{\partial\, p}{\partial\, z} \approx -\rho\, g$$

Where p is pressure, g is the acceleration of gravity, z corresponds to the vertical direction, and ρ is density.

Because of the rotation of the planet, the direction of the horizontal wind depends on the geostrophic balance between the Coriolis force, which determines its deflection, and the pressure gradient force, which appears when a pressure difference occurs across a region. This balance allows the wind to move in any direction instead of just following a circle. Moreover, the balance applies only to those regions of the planet where the rotation is dominant as the high latitudes. The geostrophic balance does not apply at the equator as the Coriolis parameter vanishes Ingersoll (2013).

The horizontal differential heating produces changes in the height of the air column. Above the warm surface, the air column is taller as warm air ascent, the opposite happens on cold surfaces, producing an inclination of the isobars (contours of equal pressure) in the vertical levels between both warm and cold regions. As the temperature decreases with height, the isobars become narrower, causing an increment in the speed of the zonal wind in height. When wind speed increases with height and temperature decrease horizontally, it is called a thermal wind Holton and Hakim (2012). Moreover, according to Reiter and Greg (2005) when the wind exceeds $10\,m/s$, it becomes a jet stream, a fluid flow that moves faster than the environment.

Fig. 2.6 shows the zonal mean wind on Earth located in the annual, DJF and JJA mean. The maximum tightening of the isobars occurs close to the tropopause ($\approx 200\,hPa$), in the location of the minimum vertical temperature. The thermal wind appears in each hemisphere, as a jet stream centered in the subtropics at $200\,hPa$ product of the ascending air from the equator and the decreasing temperatures toward the poles. The core of the jet stream appears where the isotherms are flattened vertically and where the masses of warm and cold air are intersected horizontally.

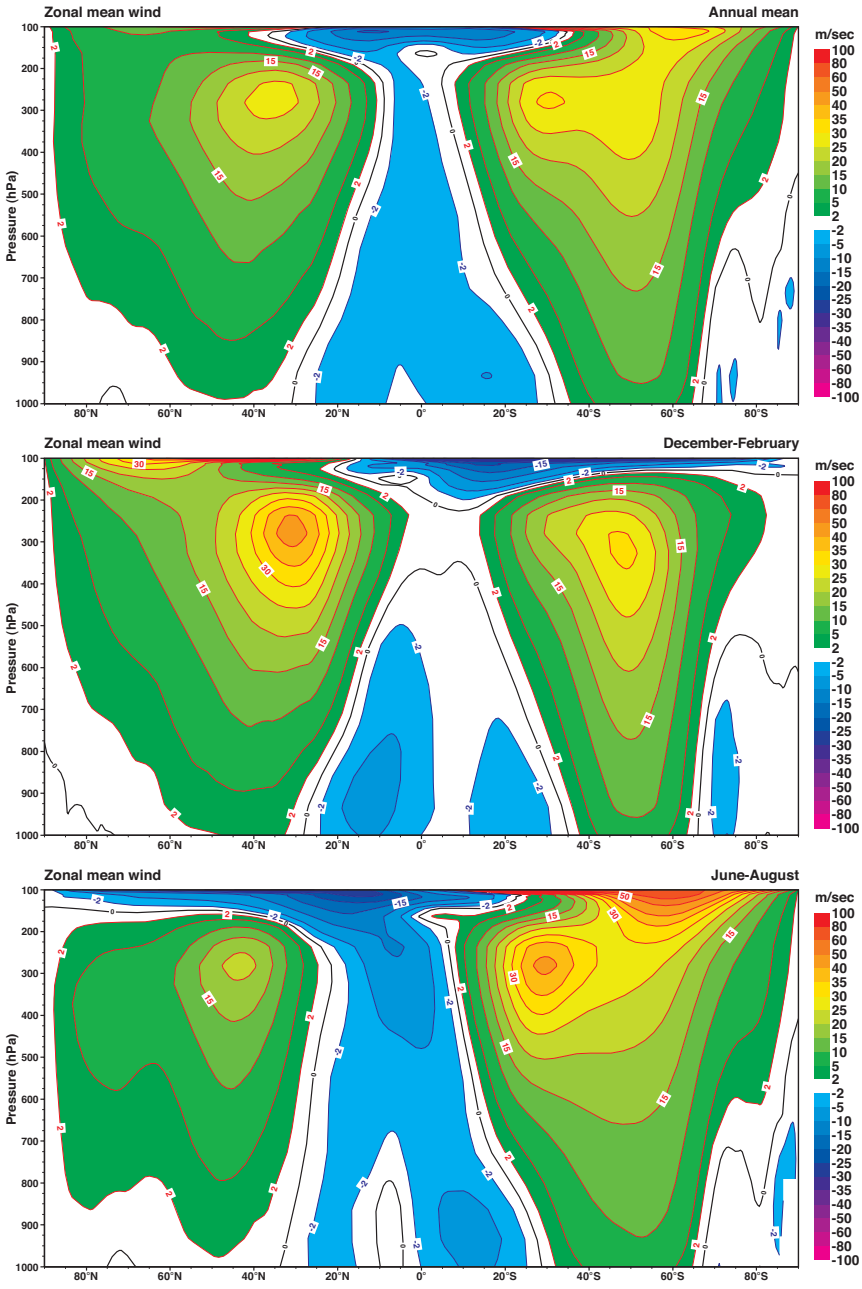

Figure 2.6: Earth's zonal wind vertical profile. The upper figure shows the annual mean; the figure in the middle corresponds to December, January and February mean (DJF, summer in the Southern hemisphere), and the bottom figure is the June, July, August mean (JJA, winter in the southern hemisphere). The development of the zonal wind is observed with greater intensity towards the maximum temperature gradient, for this reason in DJF the jet present higher intensity in the Northern hemisphere, in contrast to JJA, where the highest intensity occurs in the southern hemisphere. The shape of the jet is not symmetric in both hemispheres due to the effect of the continents towards the Northern hemisphere, and the effect of the large ocean surface towards the southern hemisphere. In the case of aquaplanets, the shape of the jet streams is expected to be similar to those observed in the southern hemisphere. (Zonal mean zonal wind - tropospheric perspective using ERA-40 Atlas from Pressure level climatologies, ECMWF, Kallberg et al. (2004)[a])

[a] https://software.ecmwf.int/static/ERA-40_Atlas/docs/section_D25/parameter_zmzwtp.html

2.3.2 Mean meridional circulation

Another effect of the differential heating of the planet's surface is the vertical movement of air masses due to convection. The air masses are heated by the surface ascending and moving towards the regions of lower temperature, on Earth, this is the North and South poles, where their temperature decreases, descending and returning to the regions of higher temperature along the surface. These convection cells extend vertically over 10 km above the surface. The warm air that ascent liberates latent heat converging near the region with the highest temperature. On Earth, this region corresponds to the Intertropical Convergence Zone (ITCZ) located in the Equatorial region, where the maximum precipitation and cloud coverage occur, associated with strong convection.

Cloud cover influences the atmospheric energetics by interacting with the incident radiation in the radiative balance, and releasing large amounts of latent heat by the condensation of water vapor available in the atmosphere (Peixoto and Oort, 1992). As indicated by Schneider et al. (2010), compared to evaporation and sublimation, the release of latent heat by condensation is more important in large scale circulation. Thus, water vapor is one of the main components in the dynamical processes of the atmospheric circulation, especially in warm climates, where the dynamical effects of air, heating or cooling by phase changes, produce the increase of atmospheric water vapor as surface temperature rises.

Moreover, the precipitation rate must be equal to the evaporation rate to avoid the accumulation of atmospheric water vapor (Wallace and Hobbs, 2006). On Earth, the ITCZ shows a higher rate of precipitation than evaporation, since there is a contribution of water vapor transported by the winds that converge in the area.

On the other hand, the cold air that is moving towards the Pole is deflected by the Coriolis force, contributing to increasing the speed of the subtropical jet stream wind. This convective circulation was first suggested by Hadley et al. (1735) who searched an explanation for the trade winds behavior. Hadley suggested the existence of a single convective cell per hemisphere that extended from the equator to the Pole, which developed as a product of the temperature difference between the two regions. Lowell (1909) proposed something similar for the Venusian convective cell regime. Nevertheless, the complexity of the circulation originates different configurations. Lorenz (1967) introduces several proposed schemes, starting with Hadley et al. (1735) single cell scheme to the breaking of this single cell creating one cell per region or even suggesting the superposition of cells in height.

It is not until the twentieth century, where it was possible to establish a configuration that explains the behavior of global winds. The model of Held and Hou (1980) states that the angular momentum per unit mass is conserved as the air parcel moves towards the pole along the ascending branch of the cell. This model allows predicting the width of the cell, which is inversely proportional to the planetary rotation rate.

On the other hand, the Held and Hou model also predicts the zonal wind velocity that exists at the top of the cell and indicates that planets with a Hadley Cell regime are only obtained when the thermal wind is comparable to the Coriolis force, measured through the thermal Rossby number (Ro_T). The condition for the planet to have at least one cell is $Ro_T \geq 1$. The Held and Hou scheme show three cells per hemisphere: the Hadley cell, with

an ascending branch located in the equator and a descending branch located in the subtropical region. The Ferrel cell whose descending branch is located in the subtropical zone and the ascendant branch; in the extratropical region. Finally the Polar cell whose ascending branch is located in the extratropical region and the descending branch in the pole.

The equation of continuity is used to describe the mass transport carried out by the meridional cells. Written in isobaric coordinates with longitude and latitude as horizontal coordinates (λ,ϕ,p,t) correspond to:

$$\frac{1}{R\cos\phi}\frac{\partial u}{\partial \lambda}+\frac{1}{R\cos\phi}\frac{\partial v\cos\phi}{\partial \phi}+\frac{\partial w}{\partial p}=0$$

Where R is the radius of the planet, λ; longitude and ϕ; latitude.

Then, by averaging over the longitudes (zonal mean), the continuity equation is rewritten as:

$$\frac{1}{R\cos\phi}\frac{\partial[\bar{v}]\cos\phi}{\partial \phi}+\frac{\partial[\bar{w}]}{\partial p}=0 \tag{2.4}$$

This equation states that both $[\bar{v}]$ and $[\bar{w}]$ can be used to define the two-dimensional flow. The Stokes current function is defined, to obtain the best representation of the flow field, which describes the current and speed lines of an incompressible flow with axial symmetry, as it is in this case.

The Stokes streamfunction which satisfies eq. (2.4) is defined as:

$$[\bar{v}]=\frac{g}{2\pi R\cos\phi}\frac{\partial\psi}{\partial p}$$

$$[\bar{w}]=-\frac{g}{2\pi R^2\cos\phi}\frac{\partial\psi}{\partial \phi}$$

Solving for ψ and integrating from the top of the atmosphere, where ψ, $p=0$, the equation for mass streamfunction is:

$$\psi(\phi,p)=\frac{2\pi R\cos\phi}{g}\int_0^p[\bar{v}(\phi,p)]\mathrm{d}p \tag{2.5}$$

Thus, the Hadley circulation corresponds to the zonal mean of vertically integrated meridional flows. Figure (2.7) shows the vertical profile of the Earth's mass stream function.

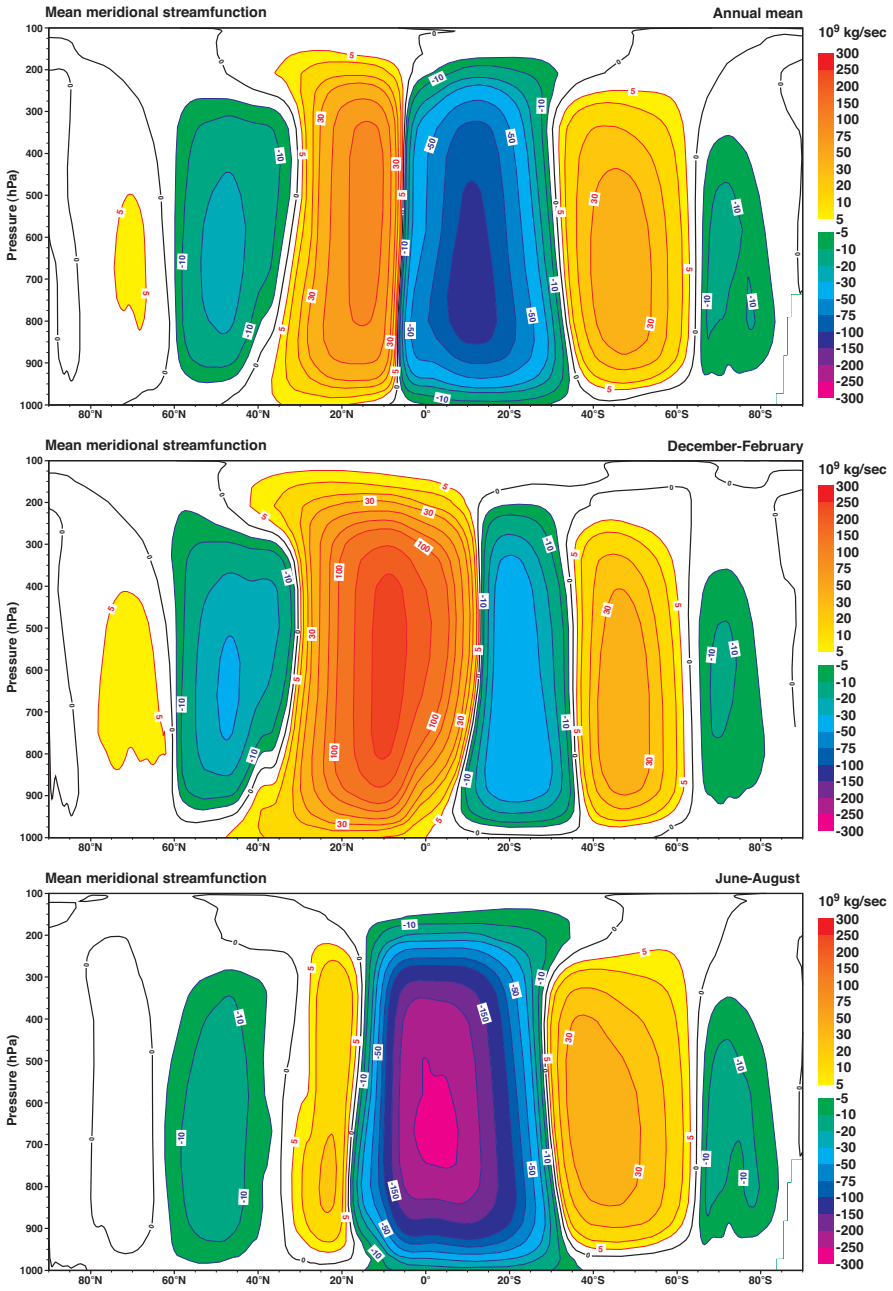

Figure 2.7: Earth's mean meridional circulation. The upper figure shows the annual mean, in the middle, the figure corresponds to December, January and February mean (DJF, summer in the Southern hemisphere) and the bottom figure is the June, July, August mean (JJA, winter in the southern hemisphere). In the annual mean, Hadley cells correspond to two cells in the Equatorial region, one in each hemisphere, Ferrel cells can be observed in the subtropics and the Polar cells are observed toward the Poles. As was indicated for the first time by Lindzen and Hou (1988), seasonally, the Hadley cell in the winter hemisphere intensify its turning, and the summer cell is almost negligible, showing a strong dependence due to thermal forcing that changes its location along the year due to obliquity. (Zonal mean meridional circulation - tropospheric perspective using ERA-40 Atlas from Pressure level climatologies, ECMWF, Kallberg et al. (2004) [a])

[a] https://software.ecmwf.int/static/ERA-40_Atlas/docs/section_D25/parameter_zmmctp.html

2.3.3 Meridional Heat Transport

As mentioned in previous sections, regions with surplus and radiation deficit cause a latitudinally radiative imbalance. The climate system compensates this difference by transporting energy (internal, potential and kinetic) from latitudes where the radiative surplus exists to those regions with a deficit of radiation.

According to Nielsen and Chen (1993) to quantify heat transport it is necessary to use a ring of defined longitude as a volume, delimited by vertical walls along two latitudinal circles that extend between the planets surface and the top of its atmosphere, allowing the atmosphere to transport energy through the wall, not above or under it. The air parcels that cross the wall do work on the air parcels that are in front of them.

Ingersoll (2013) indicates that the direction of the net energy transport will be defined by the amount of energy and work performed by the air parcel. On Earth, the net energy transport moves towards the Pole, since the air parcel retreating from high latitudes returns with less energy and doing less work to low latitudes (see Figure 2.8). Moreover, the transport of energy will be represented by different mechanisms depending on the latitude, so in the tropics, Hadley's circulation is the main responsible for the transport of atmospheric heat to the Poles, while in high latitudes transport is carried out through eddies that arise due to baroclinic instability.

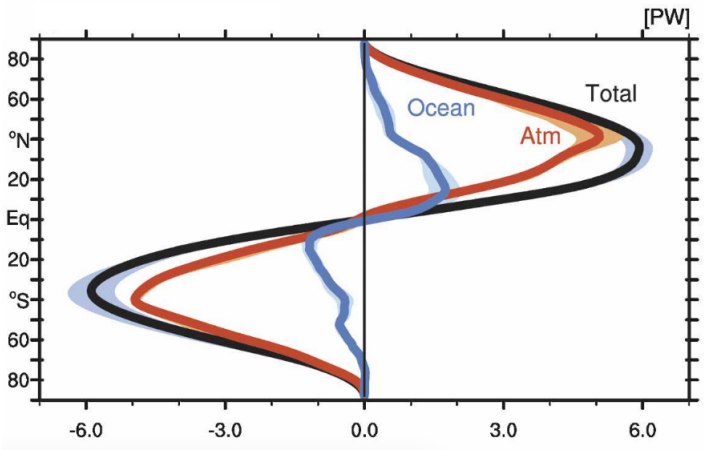

Figure 2.8: Earth's total meridional heat transport. The figure shows two amplitudes. The heat transported to the South pole appears in negative values and the heat transported to the North pole appears in positive values. The maximum value of MHT on Earth is about 6 PW between ocean and atmosphere. The black line indicates the total meridional heat transport. Red line shows the atmospheric heat transport and the blue line shows the oceanic heat transport. (From Fasullo et al., Journal of Climate, vol. 21, no 10, p. 2313-2325, 2008. With permission)

Indicated by Vonder Haar and Oort (1973), the total meridional heat transport (MHT) can be obtained by the integration of the net radiation surplus over the tropics when the planet is in radiative balance. This method corresponds to the integration of the horizontal difference (Pole to Equator contrast) between the absorbed and outgoing radiation at the top of the atmosphere. Integrating the net radiation at the top of the atmosphere over latitudes;

the total transport of energy between surplus and deficit regions can be calculated over the ocean-atmosphere system.
Following Donohoe and Battisti (2012), the total meridional heat transport at the top of the atmosphere is:

$$MHT(\phi) = -2\pi R^2 \int_{x=\sin(\phi)}^{1} [ASR(x) - OLR(x)]\,\mathrm{d}x \tag{2.6}$$

Where ϕ is latitude and R is the planet's radius, $ASR(x)$ is the absorbed solar radiation and $OLR(x)$ is the outgoing long-wave radiation, both radiations quantified at the top of the atmosphere.

As indicated by Donohoe and Battisti (2012) the maximum MHT occurs at the intersection of the latitudinal distribution of ASR and OLR ($ASR = OLR$). For this reason, when the maximum MHT varies, it is possible to infer the changes in the latitudinal net radiation contrast on the planet, especially between the higher and lower temperature zones.

Although it is important to highlight the mechanisms that compose heat transport, it is not part of the objectives of this thesis to characterize its components. Moreover, as the primary interest comes from the study of exoplanet atmospheres, this thesis will use MHT calculated from the top of the atmosphere as the methodology with a significant advantage in the extrasolar planetary study, since radiation is the only information obtained from those planets.

Chapter 3

Methodology

This chapter presents the configuration used in the general circulation model to perform the simulations. Moreover, this section presents the definitions used to analyze the experiments, including the equator to pole difference, the precipitable water vapor content and the wet bulb temperature. Furthermore, equations (2.5) and (2.6) are used to calculate the mean meridional circulation and the meridional heat transport, respectively.

3.1 Model setup

The simulations in this thesis were performed using an atmospheric general circulation model (AGCM). According to Satoh (2013), an AGCM is a numerical model that allows calculating the global atmospheric flows by using the primitive hydrostatic equations, derived from Eqs. (2.1), (2.2), (2.3), with continuity and thermodynamic equations, assuming vertical hydrostatic balance. Many AGCMs use these equations transformed in σ coordinates, since σ (vertical pressure normalized by the surface pressure), allows to incorporate topography easily.

In general, these models reach a resolution of 100 km in the horizontal. Thus with an aspect ratio of 1/100 between vertical height scale and horizontal scale movement. It is possible to represent the atmospheric movement assuming hydrostatic balance. Although these models achieve a reasonable approximation of large-scale motions, the most significant uncertainty is given by the parameterization of cumulus convection. Convection with an extension of 1 km is treated statistically, difficulting its parameterization.

The simulations of this thesis were performed using *Planet Simulator* (PlaSim, v16.022, Fraedrich et al., 2005). PlaSim is an AGCM whose dynamic core solves the fundamental hydrostatic equations using a spectral transform method, which allows calculating non-linear terms of the equations in a shorter time. The interaction of radiation with the atmosphere, formation of clouds, in addition to vertical and horizontal diffusion, are parameterized Lucarini et al. (2013).

PlaSim is an intermediate complexity AGCM because it includes sea-ice-atmosphere interaction and a slab ocean with a fixed depth, allowing the formation of sea ice but excluding the transport of oceanic heat and the drift of sea ice due to the wind. Despite this exclusion, PlaSim can use a mixed layer flux correction to model the oceanic heat flux of the slab ocean. This feature optimizes the time of numerical calculations, allowing to explore a full gamma of variables without increasing the computation time. Another advantage of PlaSim is its open source code [1] and its compatibility with NetCDF files, this is the format of the file that we can obtain after processing the output of the model by command line.

This thesis uses PlaSim to perform sixteen Earth-like aquaplanets simulations with current Earth atmospheric composition and one current Earth simulation used to make a habitability comparison in section (4.5.1). The simulations were performed with spatial resolution T42 ($2.8° \times 2.8°$) using 10 vertical levels from 1000 hPa to 100 hPa (from the surface to the lower stratosphere). Additionally, a slab ocean of $50\,m$ depth with mixed layer flux correction to simulate the oceanic heat flux of the slab ocean.

PlaSim reads the initial conditions from *namelist* files, where parameters can be modified globally: ice_namelist, land_namelist, ocean_namelist, puma_namelist, sea_namelist (see in Appendix A the values used in the simulations). Boundary conditions are initialized using $\star$.sra files which depend on the resolution. These configuration files modify oceanic albedo, sea surface temperature (SST) and continental distribution. The format of $\star$.sra files for albedo and land-sea mask, corresponding to a zonal map, where latitudes and longitudes depend on the resolution. SST configuration file is also a zonal map stored as 14 monthly fields, where January to December correspond to months 1 to 12 with December duplicated as month 0 and January duplicated as month 13 [2].

To create the aquaplanet simulation, we replace the Earth's continental distribution in the configuration files by a homogeneous land mask. Then we set the albedo at 0.06 to obtain a liquid ocean surface, as it is indicated by (Payne, 1972). Several steps and experiments were required to determine the final SST distribution of the aquaplanet. First, we determine the SST of the aquaplanet by using a high-resolution simulation (T42) of the Earth, where we identify one longitude with fewer latitudinal topographic influence. Figure (3.1a) shows the distribution of SST extracted from the Earth's simulation. Since the extracted distribution presents latitudinal variations, we made a polynomial fitting from this data:

$$\begin{aligned} SST_{fit}(\phi) = {} & 2.9 \times 10^{-16}\phi^9 - 2.226 \times 10^{-14}\phi^8 - 6.019 \times 10^{-12}\phi^7 + \\ & 3.09 \times 10^{-10}\phi^6 + 4.054 \times 10^{-8}\phi^5 - 4.289 \times 10^{-7}\phi^4 \\ & - 8.313 \times 10^{-5}\phi^3 - 0.008906\phi^2 - 0.03675\phi + 302.5 \end{aligned} \tag{3.1}$$

where ϕ corresponds to the latitude and SST_{fit} is the fitted value of SST.

Figure (3.1b) shows the distribution of SST_{fit} generated with the polynomial fitting. We use this distribution to create our first simulation of an aquaplanet with 23.5° of obliquity. However, the result was an aquaplanet in snowball state when the simulation converged.

[1] Available at https://www.mi.uni-hamburg.de/en/arbeitsgruppen/theoretische-meteorologie/modelle/plasim.html

[2] https://www.mi.uni-hamburg.de/en/arbeitsgruppen/theoretische-meteorologie/modelle/sources/psreferencemanual-1.pdf

Dahms et al. (2012) indicates the freezing point of an aquaplanet simulated with PlaSim occurs when $SST = 271.25\,K$. To avoid this snowball state, we perform a third SST distribution using the polynomial fitting from Eq. (3.1), but fixing $SST = 273.5\,K$ in the polar regions (see Figure (3.1c)) this ensures no sea ice cover in the initial conditions. This SST distribution is kept constant throughout the year as an initial condition. Even when this third SST distribution did not eliminate the snowball state in the aquaplanet with obliquity 23.5°, we use it as the initial condition of SST in our simulations, because it is a slightly more realistic version of the SST distribution proposed by Neale (2000) to simulate aquaplanets. Aquaplanets have been the model used in previous high obliquity climate research; for this reason, this SST distribution is the more appropriate for this type of experiments Satoh (2013). This SST above 0°C at poles ensures that ice will only form as a result of atmospheric dynamics and not because of the initial conditions of the simulation. At a first approach the explanation points to the oceanic heat transport mechanism, additional analysis is required to explain this phenomenon.

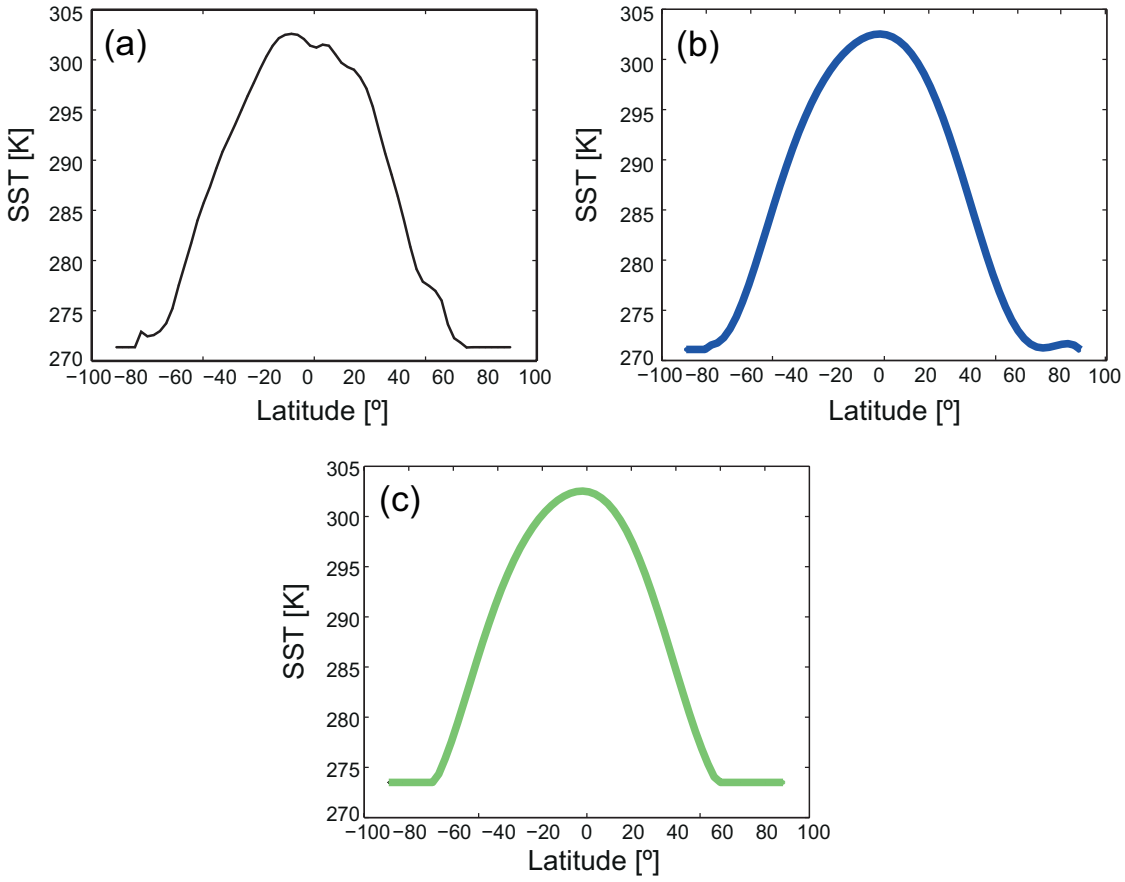

Figure 3.1: Latitudinal distribution of SST to perform the aquaplanet simulations. (a) shows the SST distribution extracted from Earth's simulation by choosing 180° longitude with fewer topographic influence, (b) shows SST distribution generated by the polynomial fitting produced with equation (3.1) and (c) shows SST generated with equation (3.1) with $SST = 273.5\,K$ in the polar regions. This SST distribution is kept constant throughout the year as an initial condition.

According to Fraedrich et al. (2005), a simulation made with PlaSim reaches its stability and convergence after 50 years. Without doing a spin-up of any particular parameter, we verify the stability of our simulations, by calculating the global mean surface temperature for each experiment in 80 years with equal months of 30 days. The last 30 years are employed to perform the climatology.

The aquaplanet at 23.5° falls into a snowball state after 40 years (see Fig. 3.2a) while the aquaplanets with $\delta \geq 30°$ shows a faster convergence that remains stable through time (see Fig. 3.2b). As the main goal of this thesis is to study warm climate aquaplanets, we select only the simulations with obliquities between 30° and 90° to avoid planets that could fall into a snowball state.

Parameters used in the experiments are shown in Table 3.1. Our aquaplanets have circular orbits (eccentricity $\varepsilon = 0$), and obliquity (δ) changes between 30° and 90° with a finer sampling around 55° (See Table 3.1).

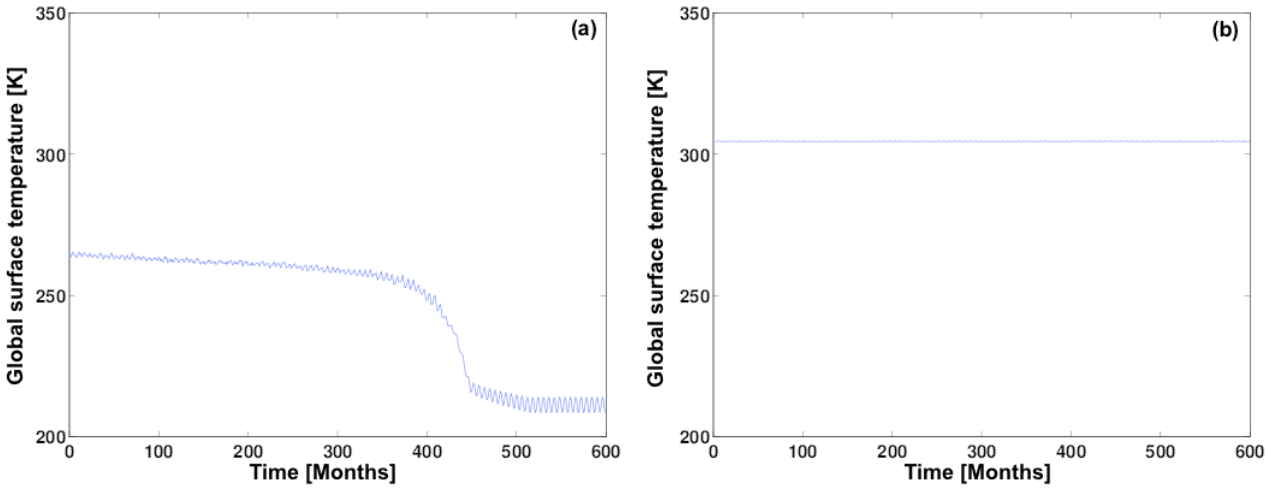

Figure 3.2: Global surface temperature time series of 50 years used to verify the convergence and stability of the simulations. The left figure shows the aquaplanet at $\delta = 23.5°$ falling into a snowball state after 40 years of an unstable simulation. The right figure shows the aquaplanet at $\delta = 80°$ where the convergence into a stable warm climate state is reached at the beginning of the simulation.

3.1.1 Definition of Equator to Pole difference

As the eccentricity is neglected, the north-south symmetry holds for all experiments (not shown). Therefore the analysis is presented for the Northern hemisphere only.

The grid of the model was used to define the polar region between latitudes 87.8°N and 71.9°N, and the equatorial region as 1.4°N and 4.2°N. This grid ensures equivalent areas $\approx 0.3\,sr$ for both regions to calculate the equator to pole differences.

Parameters	Symbol	Value	Units
Planet's radius	R	6300	km
Acceleration of gravity	g	9.8	m s^{-2}
Obliquity	δ	$30, 40, 45, 47.5,$ $50, 52.5, 54, 55,$ $57, 57.5, 60, 62.5,$ $65, 70, 80, 90$	degrees
Eccentricity	ε	0	
Ocean depth		50	m
Simulation length		80	years
CO_2 concentration		360	ppm
Solar constant	S_0	1365	W m^{-2}
Albedo		0.06	
Distance from star		1	AU

Table 3.1: Model parameters used in simulations.

ΔR is defined as the insolation difference:

$$\Delta R = R_{\text{eq}} - R_{\text{pol}}, \tag{3.2}$$

where R_{eq} is the insolation of the equatorial area, and R_{pol} is the insolation of the polar region. Both regions correspond to the latitudinal bands previously defined. ΔT is defined equivalently for surface temperature differences.

3.1.2 Precipitable water vapor content

Precipitable water vapor content corresponds to the amount of water vapor available in a vertical column. Stephens (1990) characterize the amount of precipitable water vapor content as a function of the global sea surface temperature, measuring both variables from Earth's satellite observations. With this data, Stephens (1990) obtains a Clausius-Clapeyron equation inferred by the data:

$$PWV = 10.82 \left(\frac{r}{1+\lambda}\right) \mathrm{e}^{a(\mathrm{SST}-288)}, \tag{3.3}$$

where PWV is the precipitable water content in $\mathrm{g\,cm^{-2}}$ and SST is sea surface temperature in K, with values above 288 K and $a \approx 0.064\,K^{-1}$. Stephens (1990) suggests $0.1 \leq r/(1+\lambda) \leq 0.3$ where r is the relative humidity and λ the atmospheric scale height divided by the scale height of the water vapor.

We use this equation as a method to examine the amount of precipitable water in the aquaplanets atmosphere depending on its sea surface temperature compared with Earth's data.

3.1.3 Wet bulb temperature

Furthermore, atmospheric humidity and air temperature play a key role for habitability as quantified by Sherwood and Huber (2010). In this research, the terrestrial habitability in a future scenario of climate change is examined, by using the wet bulb temperature (T_{w}), which corresponds to the lowest temperature that can be reached by evaporating all its moisture (North and Erukhimova, 2009).

T_{w} is calculated from air temperature and relative humidity by using the empirical expression presented by Stull (2011) given by:

$$T_{\mathrm{w}} = T\ \mathrm{tg}^{-1}(0.151977\,(RH\% + 8.313659)^{1/2}) + \mathrm{tg}^{-1}(T + RH\%) - \mathrm{tg}^{-1}(RH\% - 1.676331) \\ +0.00391838\,(RH\%)^{3/2}\,\mathrm{tg}^{-1}(0.023101\,RH\%) - 4.686035 \tag{3.4}$$

Where $RH\%$ correspond to the relative humidity value in % and T correspond to air temperature in $^{\circ}C$.

Chapter 4

Results

In the following sections, we analyze the atmospheric variables that determine the habitability of a planet. We evaluate these variables in the Northern hemisphere using the meteorological definition for each season as a three months period: summer as June, July, August mean (JJA) corresponding to the period of time when the northern hemisphere faces the star and winter as December, January, February mean (DJF), as the period of time when the southern hemisphere faces the star. We also use the average of the 12 months as the annual mean (ANN).

4.1 Incoming solar radiation distribution

The obliquity changes the latitudinal distribution of solar radiation at the top of the atmosphere. On Earth, poles and equator receive a different amount of solar radiation through the year. In order to compare the incident radiation in both regions, we use the equator to pole difference of the incident radiation at the top of the atmosphere (ΔR) defined by Eq. 3.2.

ΔR decreases when obliquity increases as it is seen in figure 4.1 where the equator to pole difference in its annual, JJA and DJF mean is presented. Seasonal variations are smallest for $\delta = 30°$, and largest for $\delta = 90°$, when the polar regions receive as much as $R_{\rm pol} = 726$ W m^{-2} during summer (compared to about $R_{\rm pol} = 374$ W m^{-2} for $\delta = 30°$). Values at the equator remain between +420 W m^{-2} (for $\delta = 30°$) to +334 W m^{-2} (for $\delta = 90°$).
On the other hand, in winter, as the obliquity increases, ΔR decreases linearly. Its value goes from +382 W m^{-2} to +280 W m^{-2}, this is about +1.7 W m^{-2} by degree of obliquity. Polar regions receive $\approx$ 0 W m^{-2} in winter maintaining the positive values of ΔR. In summer, ΔR decreases at a larger rate going from +46 W m^{-2} to −392 W m^{-2}.
The equator receives more insolation than the polar region for obliquities below $\delta = 54°$ in the annual mean. Above this obliquity, the polar regions get more insolated. At $\delta = 54°$, poles and equator receive nearly the same amount of insolation in the annual mean, presenting a nearly flat latitudinal distribution of the insolation in the annual mean. Seasonally at $\delta = 54°$, ΔR goes from −208 W m^{-2} in summer to +335 W m^{-2} in winter.

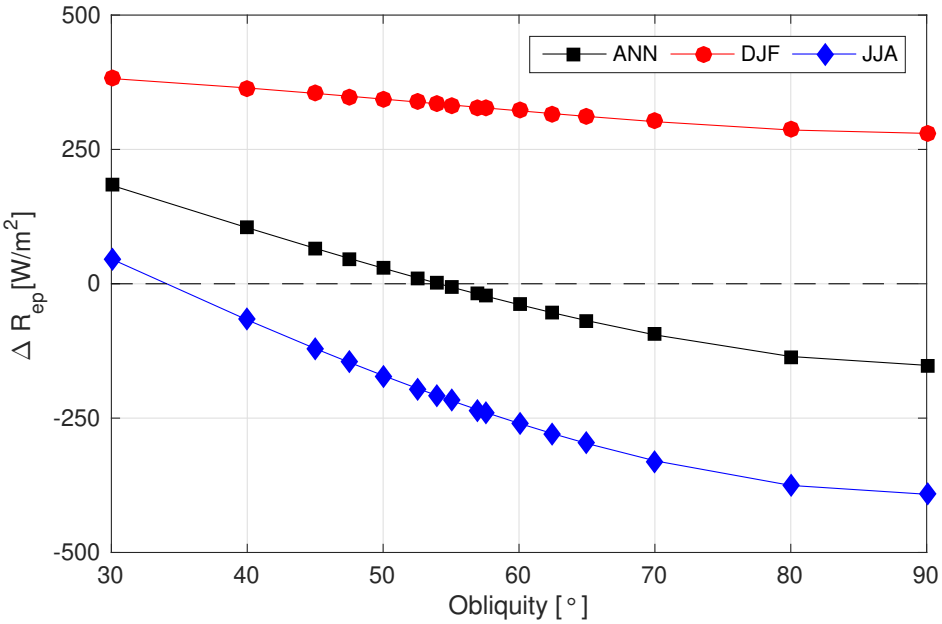

Figure 4.1: Equator to pole difference of incoming solar radiation at the top of the atmosphere for each obliquity. Black, red and blue symbols correspond to annual mean, DJF, and JJA means, respectively. Positive values indicate higher insolation at the equator.

Section 2.2.1 presented the interaction between solar radiation and the atmosphere. Solar radiation is absorbed, reflected and scattered by the atmospheric compound as it moves towards the surface. This interaction presented in Figure 4.2 shows the total amount of solar radiation partitioned into three components: Absorbed Solar Radiation at the surface (ASR), Absorbed Solar Radiation in the atmosphere (ASRa) and Outgoing Solar Radiation at the top of the atmosphere (OSR). We have represented these three variables, as areas, giving us an estimation of some processes that can be affecting the radiative balance; as the presence of clouds or the surface albedo. Figure 4.2 shows the balance between ASR, ASRa, and OSR, maintaining a constant incident solar flux at the top of the atmosphere when obliquity increases.
For $30° \leq \delta \leq 52.5°$ the mean values of ASR, ASRa and OSR are constant: 175 $\mathrm{W\,m^{-2}}$, 250 $\mathrm{W\,m^{-2}}$ and 90 $\mathrm{W\,m^{-2}}$ respectively. Indicating the changes in the partitioning of solar radiation are not a clear function of obliquity.
Oceanic albedo, with its low reflectivity, allows most of the solar radiation to be absorbed by the surface (ASR), as seen in the blue area of figure 4.2. When the obliquity increases, ASR changes from 175 $\mathrm{W\,m^{-2}}$ to 187 $\mathrm{W\,m^{-2}}$.

Clouds

The areas of ASRa and OSR, green and yellow respectively in figure 4.2, have similar size because the cloud cover (CC) is about 50%, reaching 54% at $\delta = 30°$ and 48% at $\delta = 90°$. ASRa increases between 73 $\mathrm{W\,m^{-2}}$ and 76 $\mathrm{W\,m^{-2}}$ and OSR decreases from 93 $\mathrm{W\,m^{-2}}$ to 78 $\mathrm{W\,m^{-2}}$. At $\delta = 52.5°$, the atmosphere increases the absorption of solar radiation. OSR starts decreasing and ASR increases. CC changes solar radiation distribution. Fig. 4.2 also shows a mean CC between 50% and 60%. The aquaplanet with $\delta = 30°$ presents the largest latitudinal and interannual variations, with a mean value of 55%.

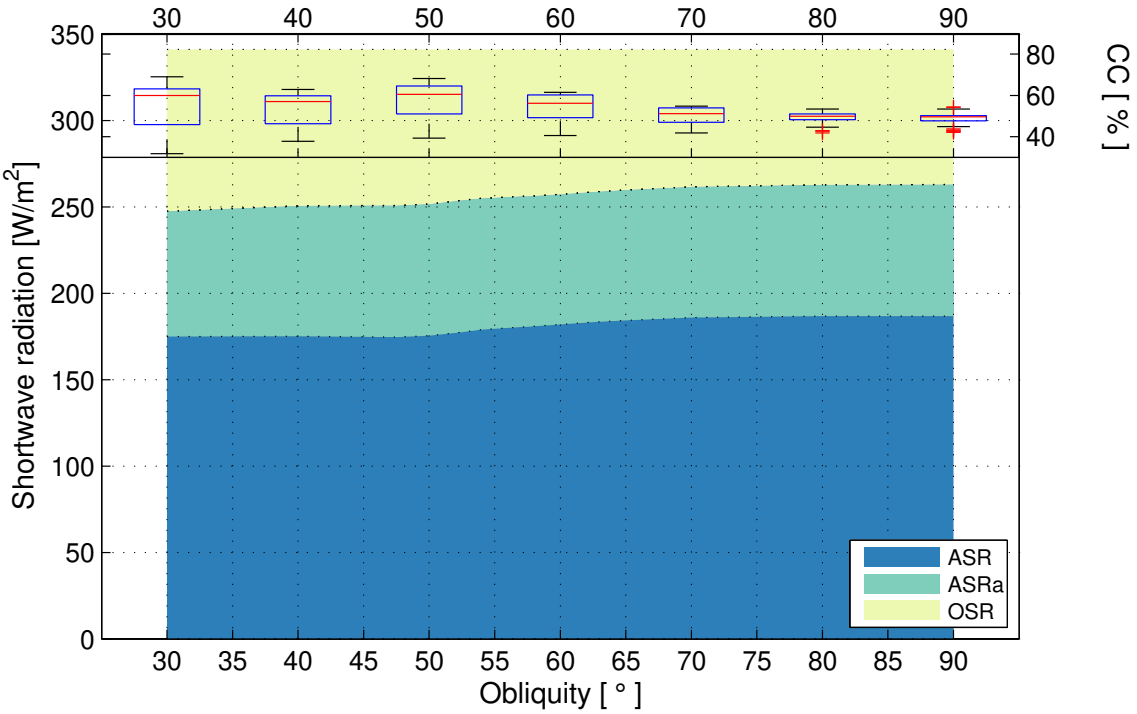

Figure 4.2: Global annual mean partitioning of solar radiation for each obliquity. Blue indicates the Absorption of Solar Radiation at the surface (ASR), green is the Absorption of Solar Radiation by the atmosphere (ASRa) and yellow is the Outgoing Solar Radiation at the top of the atmosphere (OSR). Boxplots show the statistics for annual mean cloud cover (CC), about its latitudinal and interannual variations.

CC then increases to about 60% for $\delta = 52.5°$. This rise in CC maintains the ASR almost constant for this obliquity range. Above 52.5° global CC decreases, reaching mean values below 50% at $\delta = 90°$.
Latitudinal and interannual variations of CC also decrease for the high obliquity aquaplanets. The reduction of CC produces smaller solar reflection and more significant absorption of solar radiation by the surface. Cloud cover decreases latitudinally and vertically as obliquity increases.

The interaction between clouds and solar radiation depends on the cloud vertical location and thickness. Figure 4.3 shows the vertical distribution of cloud cover in the JJA mean. In general, the aquaplanets present a maximum cloud coverage in the winter hemisphere, with low-level (850 hPa) and high-level (200 hPa) clouds. Low and middle-level (500 hPa) clouds are predominant in aquaplanets with $\delta = 30°, 45°$ (see figures 4.3a and 4.3b). As the obliquity increases, mid-level clouds cover decreases, and high-level clouds cover the winter hemisphere and the equatorial region inclined toward the summer hemisphere (see figures 4.3c and 4.3d).

As the obliquity increases, cloud cover decreases globally, with thinner low-level and high-level clouds concentrated mostly in the winter hemisphere. Clouds reflect incident solar radiation, by reducing the cloud coverage, more solar radiation reaches the surface. As the ocean has a low albedo, the surface absorbs the solar radiation, increasing its temperature.

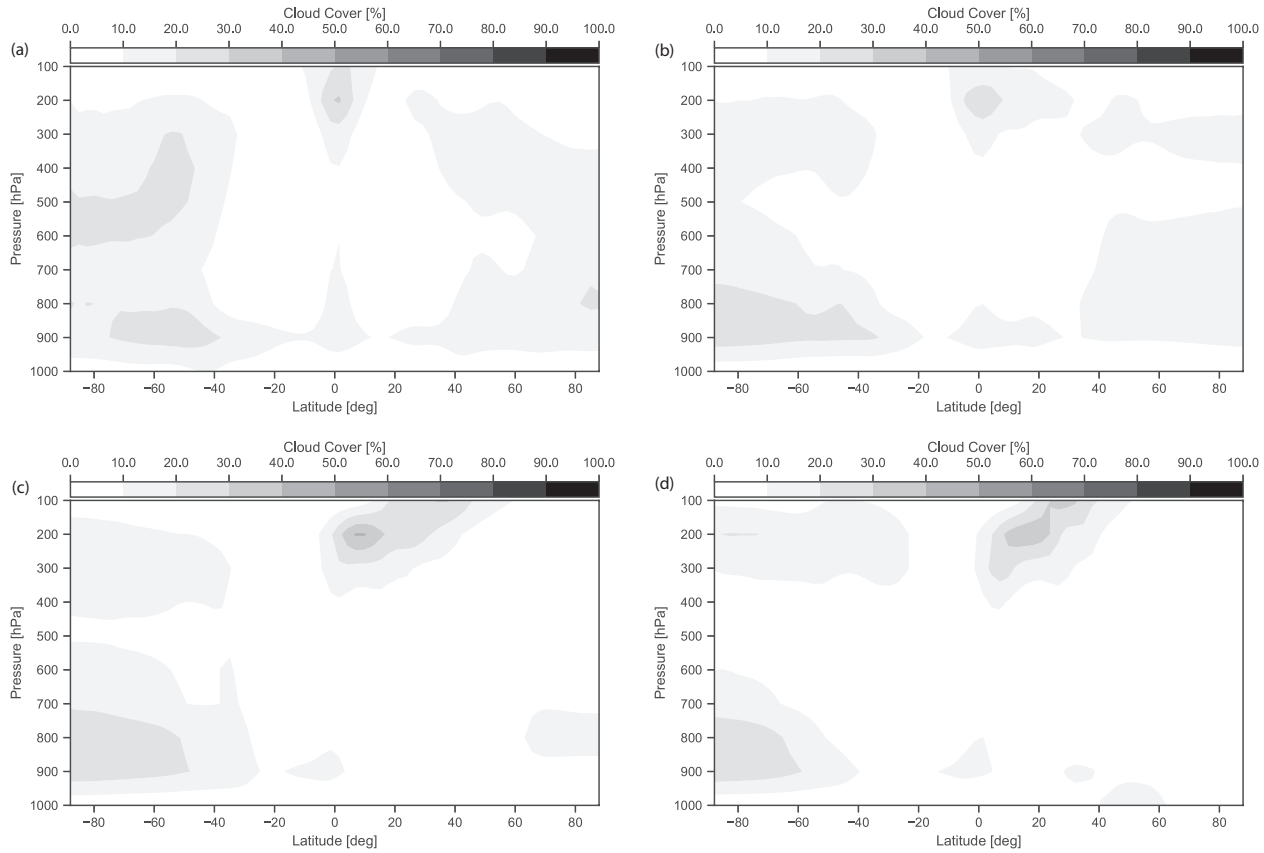

Figure 4.3: Vertical profile of cloud cover (%) in JJA for aquaplanets at (a) $\delta = 30°$, (b) $\delta = 45°$, (c) $\delta = 60°$, (d) $\delta = 90°$.

4.2 Global mean surface temperature

A direct effect of raising the obliquity is an increase in the global mean annual surface temperature (T_{glob}). Fig. 4.4 shows a mere 9 K increase in the global temperature for such significant obliquity variations, suggesting that both the ocean and the atmosphere are very efficient in redistributing the incoming solar radiation. We observe this especially in aquaplanets with high obliquities because they have surface temperatures above freezing throughout the year even when the insolation produces strong seasonal variations as the winter hemisphere is in complete darkness.

Latitudinal and interannual variations from the mean T_{glob} are largest at $\delta = 30°$ (boxplot in Fig. 4.4), decreasing gradually towards $\delta = 52.5°$. T_{glob} changes with obliquity following the empirical expression:

$$T_{\text{glob}} = -1.55 \times 10^4 \, \delta^{-2.2} + 305.5 \tag{4.1}$$

where T_{glob} is the annual global surface temperature in K and δ represents the obliquity in degrees.
The total amount of solar radiation arriving at the top of the atmosphere does not vary in our experiments, but it is the latitudinal distribution that changes. We will discuss this in the following section.

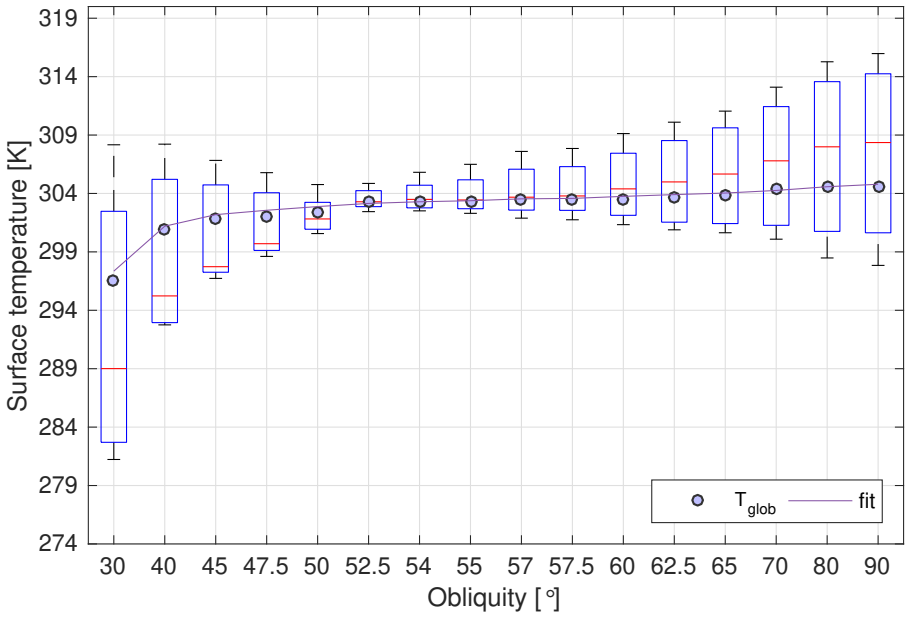

Figure 4.4: Global mean surface temperature for each obliquity. Boxplots show variations in latitudinal distribution and interannual variability of surface temperatures. Red line corresponds to the median of the data, grey dots shows T_{glob}. Box extremes correspond to the lower and upper quartile. Whiskers show minimum and maximum values. Grey line is the fitting curve for T_{glob} given by Eq. 4.1. Note that the distance between boxplots is not linear.

4.3 Latitudinal distribution of surface temperature

Polar amplification and temperatures above freezing are the main features in the latitudinal distribution of annual mean surface temperature (T_{s}) as the climate changes from cold to warm poles (see Fig. 4.5). We identify two regimes with similar behavior delimited by $\delta = 52.5°$. Below this obliquity, the equator is warmer than the poles. Over $\delta = 52.5°$ polar regions are warmer, as one would expect from the insolation distribution. The annual mean temperature has a constant value of 302 K at latitudes $\pm 30°$, except in the aquaplanet with $\delta = 30°$, which is colder at these latitudes. We observe the smallest latitudinal temperature gradient in the aquaplanet with $\delta = 52.5°$, although at $\delta = 54°$ the latitudinal insolation curve is flat (see Fig. 4.4).

Surface temperature between Equator and Poles range between 303.7 K and 305.8 K at $\delta = 54°$; 302.1 K to 309 K at $\delta = 60°$ and 297.8 K to 316 K at $\delta = 90°$. Comparison with previous studies indicates these surface temperatures have a similar range as Linsenmeier et al. (2015) when $\delta = 60°$ and 90°, but are higher in our case than Ferreira et al. (2014) when $\delta = 54°$ and 90°.
Fig. 4.6 shows that the largest ΔT is found for $\delta = 30°$, for both the annual and seasonal means. ΔT decreases towards zero for $\delta = 52.5°$, and increases again for higher obliquities. $\Delta T = 0$ K occurs in the annual mean at $\delta = 52.5°$ and seasonally at $\delta = 47.5°$ (summer) and $\delta = 57.5°$ (winter), thus are the planets with the weakest synoptic scale atmospheric activity.

With increasing obliquity, ΔT does not decrease linearly as in ΔR, instead ΔT decreases at a larger rate. Comparing $\delta = 30°$ with $\delta = 90°$, ΔT decreases 59% in winter, increases 18% in summer and decreases by 33%, annually. $\Delta T < 0\,\mathrm{K}$ indicates that the poles are warmer than the equator.

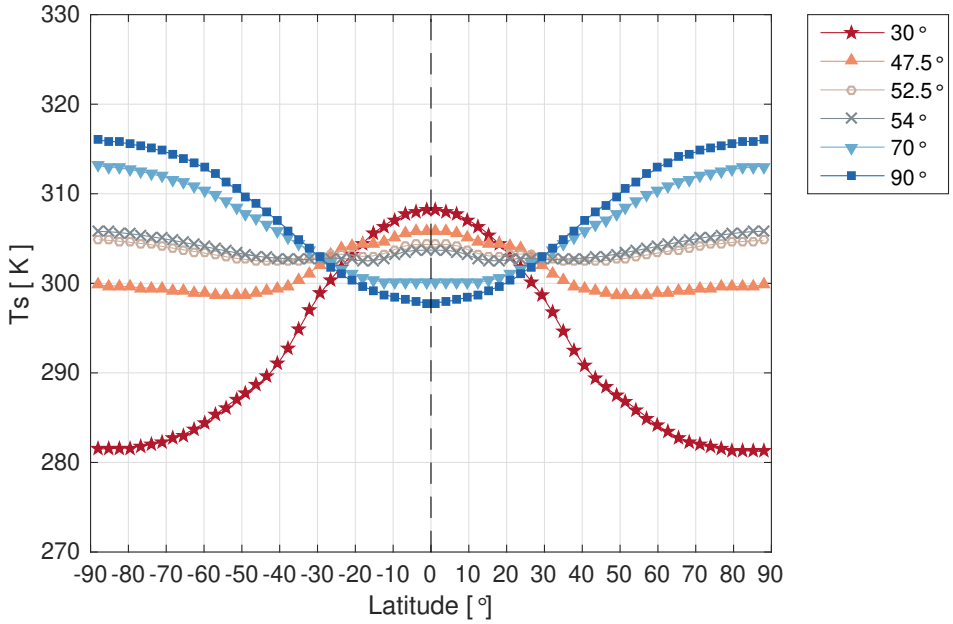

Figure 4.5: Latitudinal distribution of the annual mean surface temperature T_s, for some representative cases of simulated aquaplanets (colour lines).

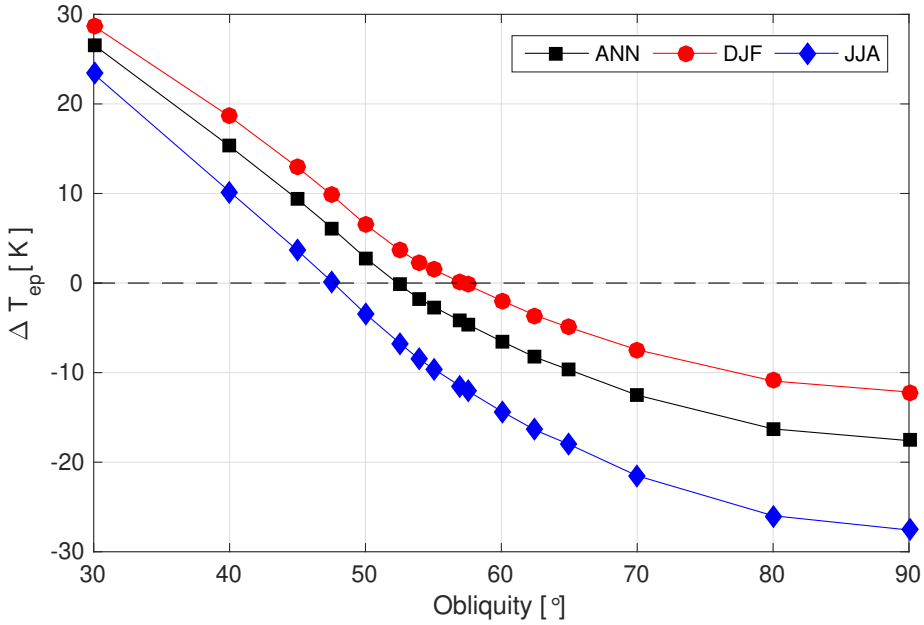

Figure 4.6: Equator to pole difference of surface temperature (ΔT) for each obliquity. Black, red and blue symbols correspond to annual, DJF and JJA means, respectively. Positive values indicate higher temperatures at the equator.

4.4 Atmospheric circulation

Differential insolation produces latitudinal temperature gradients in the atmosphere that are in thermal gradient balance with zonal westerly winds. The tropospheric temperature and wind structures sustain the large scale atmospheric overturning circulation (Hadley cells; Held and Hou, 1980), associated baroclinic instabilities and storm-tracks that transport heat from warmer to colder regions in the atmosphere.

As the obliquity increases, the latitudinal distribution of temperature changes not only on the surface but also in vertical levels. Figure 4.7 shows the vertical profile of the temperature anomaly for the JJA mean, at the obliquities 30°, 45°, 60° and 90°. The temperature anomalies are calculated as the difference between the total average of the temperatures for the obliquity set, minus a particular obliquity value, to highlight the changes in temperature distribution as the obliquity increases.

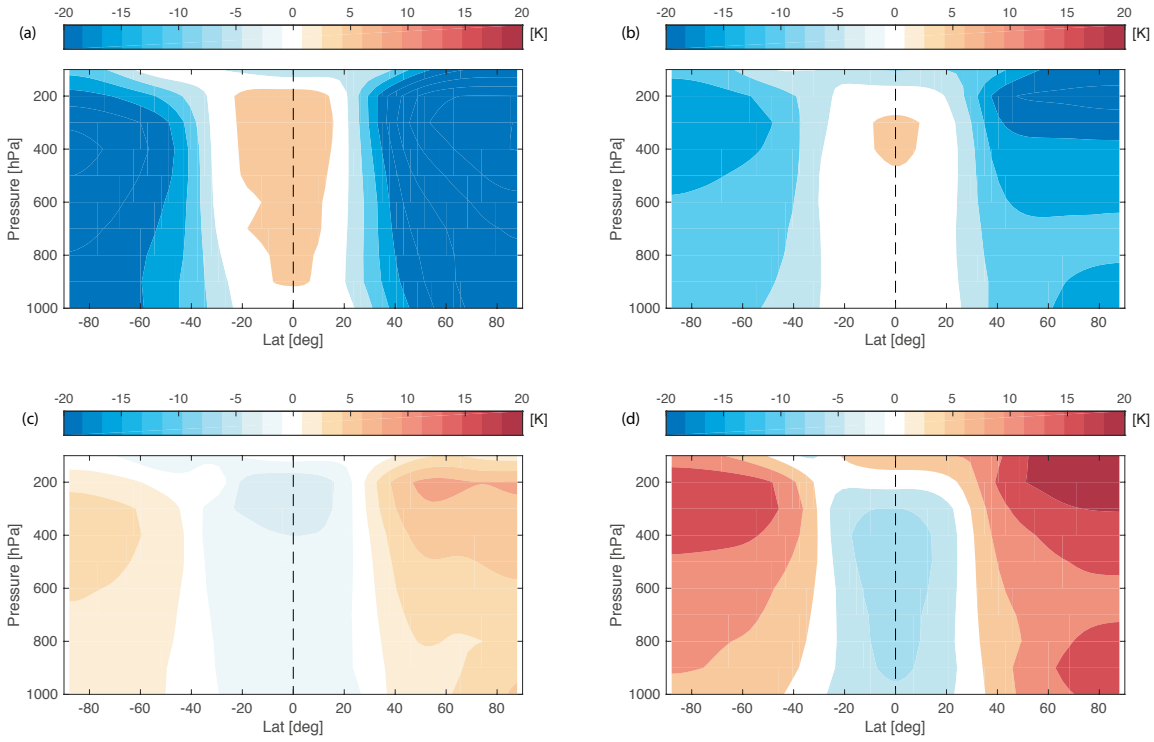

Figure 4.7: Vertical profile of temperature anomaly in JJA mean for aquaplanets at obliquities: (a) $\delta = 30°$, (b) $\delta = 45°$, (c) $\delta = 60°$ and (d) $\delta = 90°$.

The equatorial region receives a higher amount of incident short-wave radiation than the polar regions at low obliquities. Figure 4.7a shows the vertical profile of the temperature anomalies of the aquaplanet at $\delta = 30°$. The temperature of the equatorial region is 5 K warmer than the total mean in vertical levels compared to the polar regions, which is 20 K colder than the total mean.
The temperature of the polar regions raises as obliquity increases. In some cases, the temperatures of the polar regions are comparable with the temperature of the equatorial regions.

Figure 4.7b shows the vertical profile of temperatures in the aquaplanet with $\delta = 45°$, the poles maintain temperatures lower than the total mean, but also the equatorial region decreases its temperature. The transition occurs at $\delta = 54°$ (see Fig. 4.5), where poles and equator have similar temperature in the annual mean.
Figure 4.7c shows the vertical profile of temperatures in the aquaplanet with $\delta = 60°$. The equatorial region presents temperatures 5 K colder than the total mean, while the polar regions increase its temperature in 10 K.
Polar regions reach their maximum temperature in the aquaplanet with $\delta = 90°$ as the temperature is up to 20 K warmer than the total mean. However, the equatorial region only decreases its temperature by 5 K below the total mean (see Fig. 4.7d) The temperature gradient favors the appearance of a strong wind nearby to latitudes $\pm 30°$, the position of the maximum horizontal temperature gradient. As can be seen in aquaplanets with obliquities below 50° (Fig. 4.8a and 4.8b). As obliquity increases, the poles start receiving more insolation than the equator in the annual mean, the temperature gradients decrease, and the jet streams decrease their intensity. At the same time, easterly winds at equatorial latitudes appear.

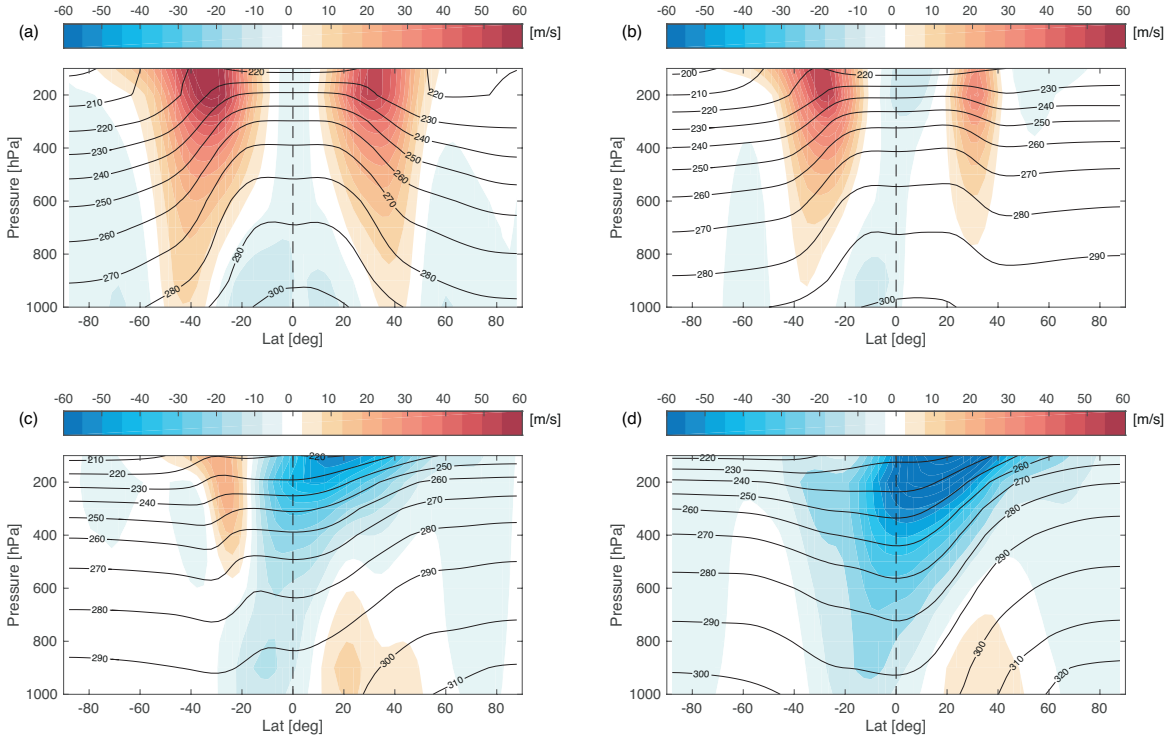

Figure 4.8: Vertical cross section of zonal wind (colors) and air temperature (contours) in JJA for aquaplanets at at obliquities: (a) $\delta = 30°$, (b) $\delta = 45°$, (c) $\delta = 60°$ and (d) $\delta = 90°$.

From $\delta = 50°$ onwards, easterly winds develop at upper levels, increasing its speed as the reversed meridional temperature gradient increases, and intruding from the summer hemisphere into the winter hemisphere (negative magnitudes in Fig. 4.8c and 4.8d). At high obliquity, the meridional temperature gradients for the winter hemisphere throughout the troposphere is small because the entire hemisphere receives little insolation from the top and is uniformly heated from below by the ocean (see Ferreira et al., 2014).

The intensity of the westerly jet stream decreases gradually by increasing the obliquity, as the development of the jet stream located at 200 hPa depends on the slope of the isotherm in vertical levels.
Fig. 4.9 summarizes the seasonal change of the intensity and position of the jet stream in the Northern Hemisphere. Above $\delta = 54°$, the poles become warmer, changing the inclination of the isotherms in vertical levels, promoting the development of an easterly jet stream in the equatorial region weakening the sub-tropical westerly jet stream. The slope of the isotherm becomes more pronounced as the temperature of the poles increases, boosting the easterly jet stream to achieve a wind speed of 67 m/s on the aquaplanet with $\delta = 90°$.
Fig. 4.9a shows how the large values in wind speed reflect the inter-hemispheric temperature gradients. Moreover, Fig. 4.9b shows the change in the position of the jet stream core, moving from the sub-tropical to the equatorial region after the inversion of the slope of the isotherms occurring above $\delta = 54°$. Vertical and meridional winds affect the overturning circulation.

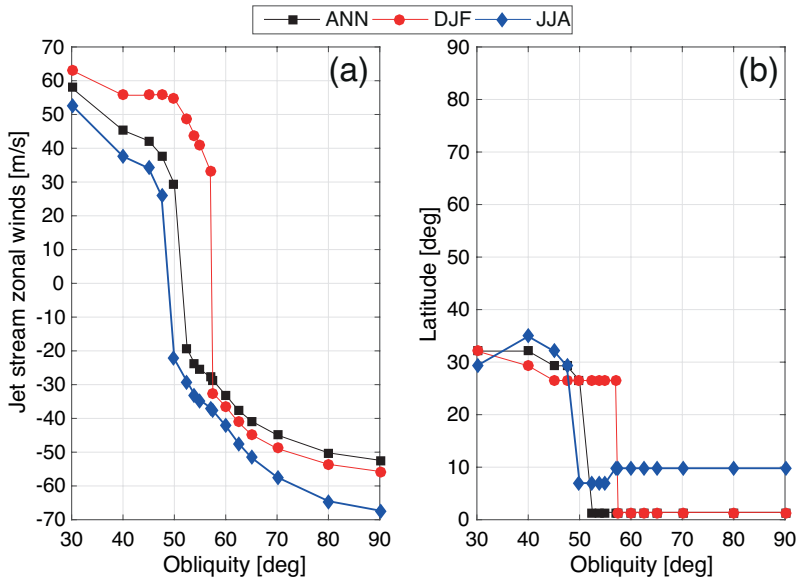

Figure 4.9: Seasonal change of magnitude and position of the jet stream at 200 hPa in the Northern Hemisphere. Figure (a) shows the maximum zonal winds speed, positive values indicate a westerly wind, while negative values indicate easterly wind, and (b) shows the position of the maximum jet stream, both figures for the annual mean (black squares), winter (DJF, red circles) and summer (JJA, blue diamond).

Figure 4.10 shows the vertical profiles of the meridional (left column) and vertical (right column) winds in height as the obliquity increases. The latitudinal distribution of meridional winds in aquaplanets with obliquities less than $\delta = 45°$ is alternated between northerly (from north to south) and southerly (from south to north) winds (see Fig. 4.10a). Above this obliquity, southerly wind prevails in the surface, reaching extratropical latitudes in the summer hemisphere. While northerly wind predominates in height, nearby the equatorial region (see Fig. 4.10c,4.10e,4.10g).

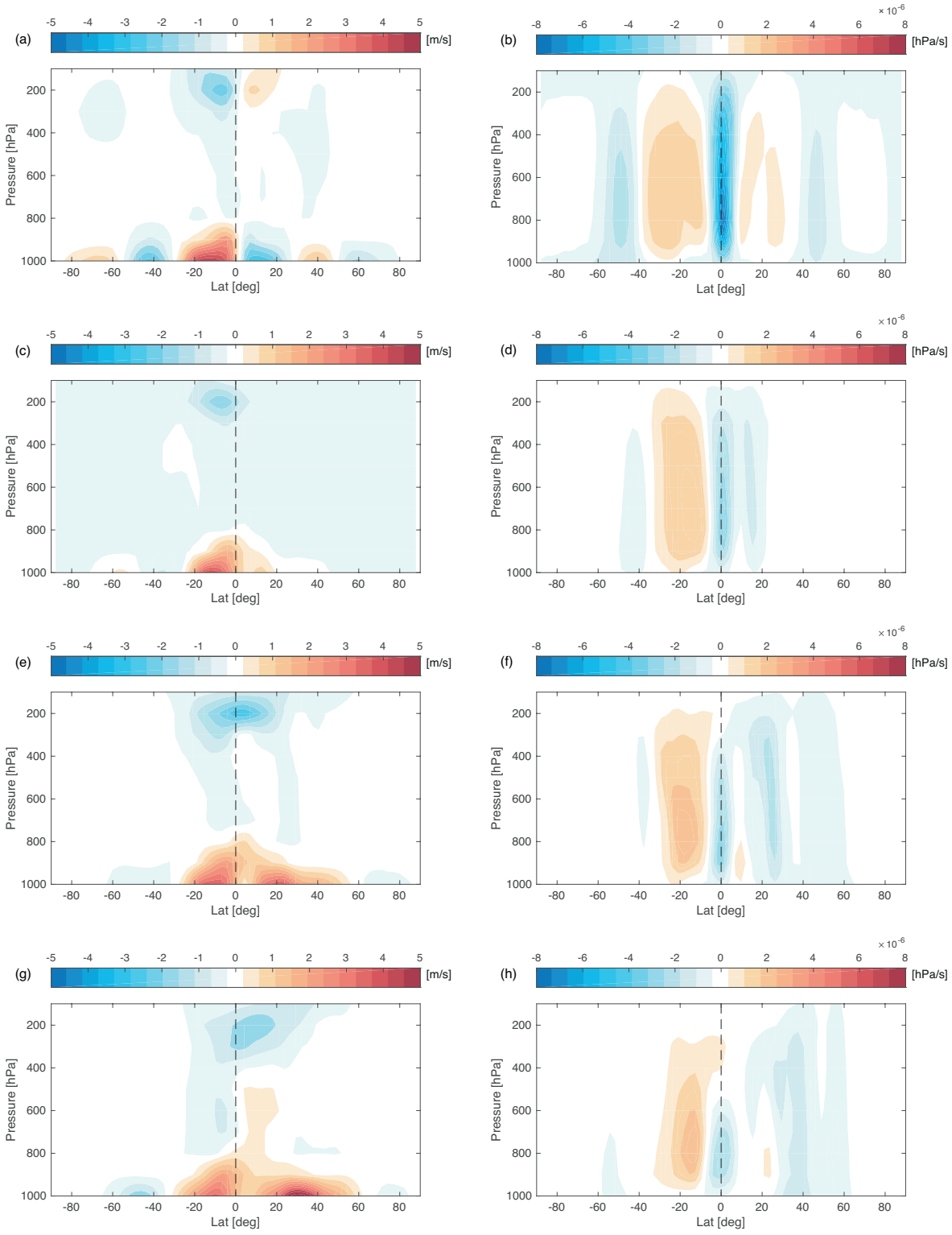

Figure 4.10: Vertical cross section of meridional and vertical winds in JJA mean. Left column shows the change of meridional wind for obliquities (a) $\delta = 30°$, (c) $\delta = 45°$, (e) $\delta = 60°$ and (g) $\delta = 90°$. Negative values (blue) indicates northerly wind (from north to south) and positive values (red) indicates southerly wind (from south to north). Right column shows the change of vertical wind for aquaplanets at (b) $\delta = 30°$,(d) $\delta = 45°$,(f) $\delta = 60°$ and (h) $\delta = 90°$. Negative values (blue) indicates ascending wind and positive values (red) indicates descending wind.

On the other hand, vertical wind decreases its intensity as the obliquity increases. In obliquities less than $\delta = 45°$, ascending winds predominate near the Equator while descending winds tend to cover a greater extension with less intensity (see Fig. 4.10b). At high obliquity values, descending winds are predominant, in the winter hemisphere (see Fig. 4.10d, 4.10f, 4.10h).

As vertical and meridional winds change, the large-scale atmospheric overturning circulation is also affected by the seasonal changes produced by the high obliquity. The seasonal Hadley cell is a thermally direct circulation predominantly in the winter hemisphere. The convective cell produces a rising motion at its equatorial flank (summer hemisphere) and the descent motion in the winter hemisphere.
Figure 4.11 shows the evolution of the mean meridional circulation by increasing the obliquity. Aquaplanets with obliquities less than $\delta = 45°$ have three cells by hemisphere, as expected by the meridional winds. Hadley cells in the winter hemisphere predominate over Ferrel and polar cells (see Fig. 4.11a). The development and intensity of the vertical wind influence the rotation of the cells.

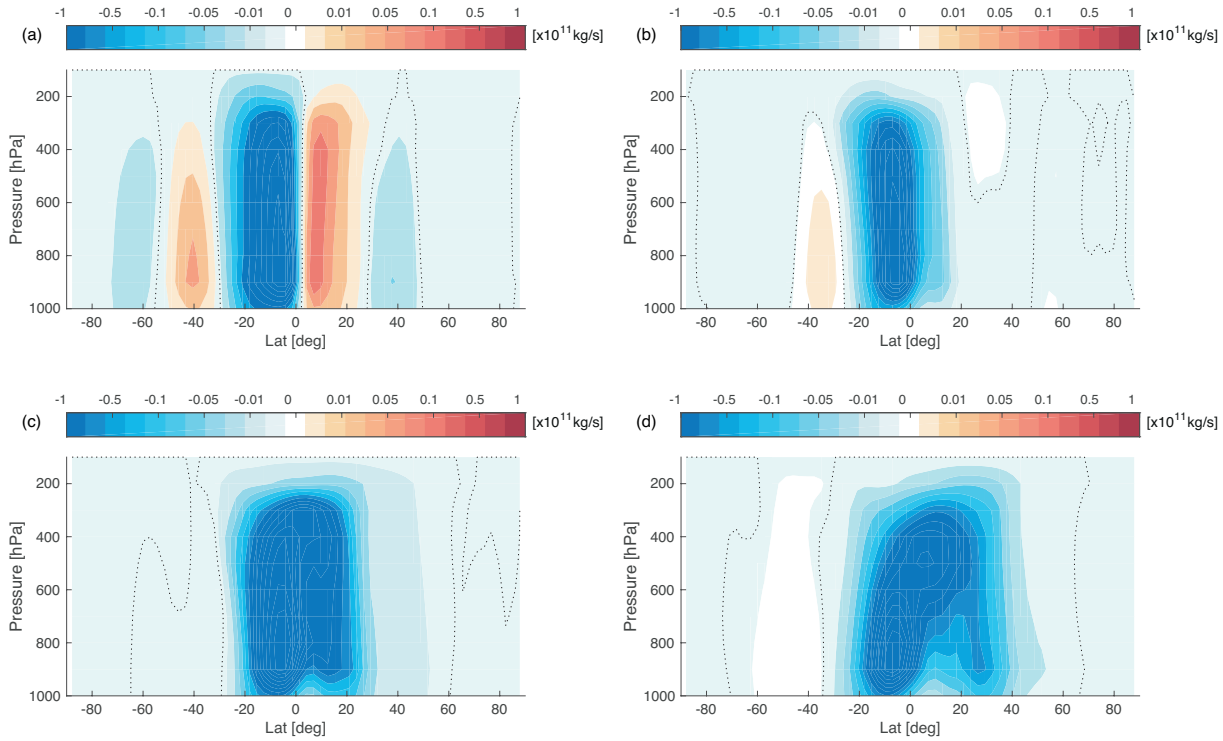

Figure 4.11: Vertical cross section of mass streamfunction in JJA for aquaplanets at (a) $\delta = 30°$, (b) $\delta = 45°$, (c) $\delta = 60°$ and (d) $\delta = 60°$ respectively. Negative values (blue) indicate counterclockwise rotation while positive values (red) indicate clockwise rotation.

Above $\delta = 45°$, one cell predominates with counterclockwise rotation (see Fig. 4.11b). Figure 4.11c shows an extended Hadley cell in the winter hemisphere besides a stronger rotation in the summer hemisphere. Its extension and intensity depend strongly on the meridional winds, due to the weakening of the vertical winds, the maximum rotation of the cell is near the surface, with a vertical inclination toward the northern hemisphere (see Fig. 4.11d).

Figure 4.12 shows a summary of the maximum intensity of the Hadley cell rotation at 500 hPa seasonally. Above $\delta = 70°$, the height of the Hadley cell decreases below 500 hPa in the annual mean. However, a narrower and weaker cell is present in the summer hemisphere. Fig. 4.13 shows the latitudinal extent of the Hadley cell at 500 hPa, depicted by the mass stream function. From $\delta = 45°$ the narrower summer hemisphere cell disappears entirely, and the primary cell becomes wider descending into the summer hemisphere. In the annual mean, the mid-latitude overturning circulation (Ferrell cells; Kuo, 1956) increases its height and moves to the equator affecting the shape of Hadley cells.

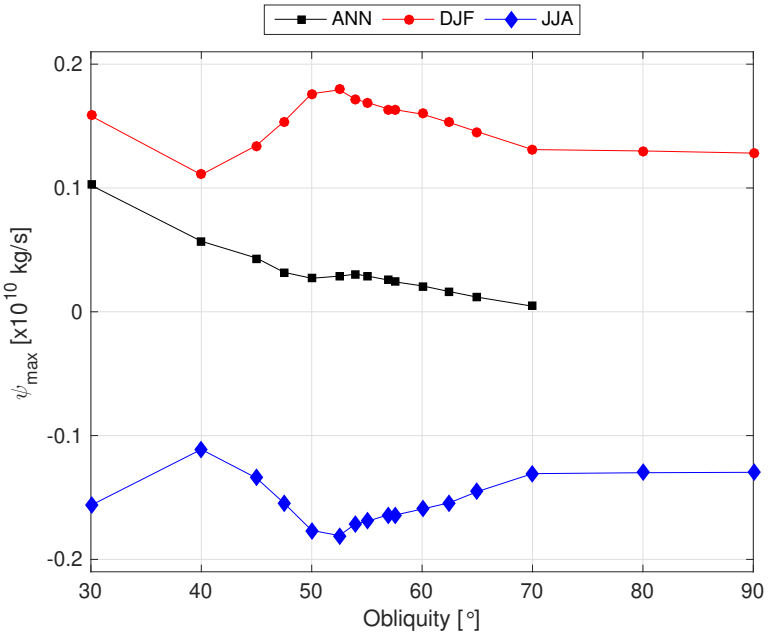

Figure 4.12: Maximum magnitude of the mass stream function at 500 hPa (depicting the Hadley cell) for each obliquity. Black, red and blue lines and symbols correspond to annual, DJF and JJA mean, respectively.

The differential heating of the surface produced by increasing the obliquity causes variations in the latitudinal and vertical extension of the meridional circulation. The Hadley cell predominates over the other convective cell seen in the aquaplanet with $\delta = 30°$. The Hadley cell turns into a counter-clockwise rotation cell with less intensity. Its latitudinal extension becomes planetary while its vertical extension decreases reaching a height lower than 500 hPa in the annual mean of the aquaplanet with $\delta = 90°$

Finally, we show the total atmospheric meridional heat transport (MHT), calculated with equation 2.6, resulting from these large-scale circulation changes in Fig. 4.15, including the latitude of the maximum MHT. Figure 4.14 shows the change in the sign of the meridional heat transport as the temperature increases at the poles, by increasing the obliquity.

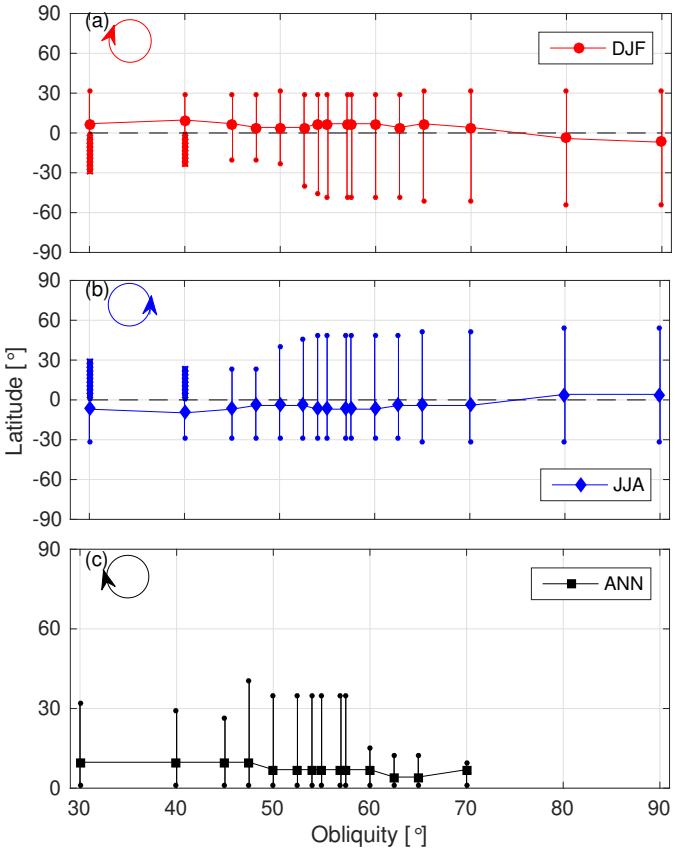

Figure 4.13: Width of mass stream function at 500 hPa depicting the Hadley Cell for each obliquity, and (a) DJF, (b) JJA and (c) annual mean. Red and thick blue lines correspond to the Hadley Cell that appears in the summer hemisphere for $\delta = 30°$ and $\delta = 40°$. The direction of turning of the cell is indicated by the upper left corner of each panel.

In the annual mean the absolute value of MHT is most significant for the aquaplanet with $\delta = 30°$, decreasing into a minimum value at $\delta = 52.5°$ and then increasing again. The direction of transport is down the temperature gradient (from warm to cold regions) and hence towards the pole for $30° \leq \delta \leq 54°$ (positive values). Then it reverses direction and moves towards the equator (negative values, Fig. 4.15ab).

For high obliquities, it is the summer hemisphere that drives heat transport. The flat meridional temperature structure in the winter hemisphere saw in previous sections reduces the winds and hence the eddy components of the heat transport. During Northern Hemisphere winter (JJA) the Southern Hemisphere transports heat into the Northern hemisphere. The largest values are near the equator (Fig. 4.15b).

MHT moves poleward to equatorward, as obliquity increases due to warmer polar regions at high obliquity. The amplitude of MHT changes depending on the temperature difference between equatorial and polar regions. The amplitude flattens in the aquaplanets with the similar equator to poles temperatures while it increases as the planet needs to maintain a global temperature balance effectively, especially where insolation is extreme in one of the hemispheres.

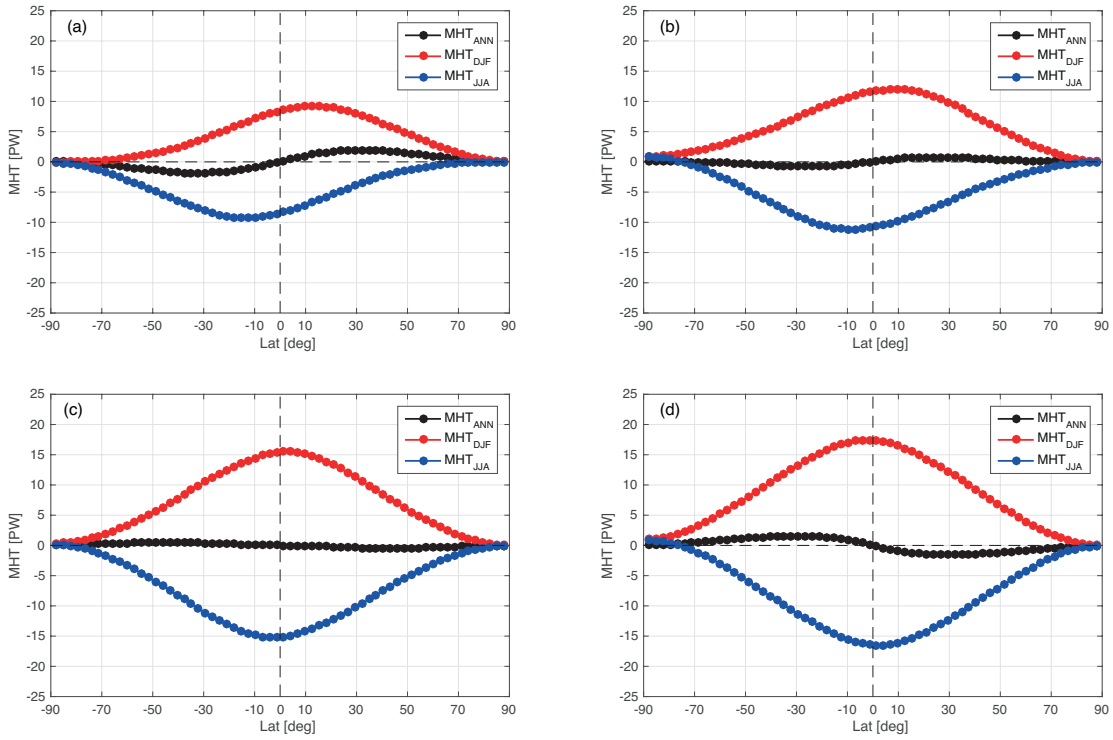

Figure 4.14: Meridional Heat Transport in the annual mean (black squares), winter (DJF, red circles) and summer (JJA, blue diamond) for obliquities (a) $\delta = 30°$, (b) $\delta = 45°$, (c) $\delta = 60°$ and (d) $\delta = 90°$.

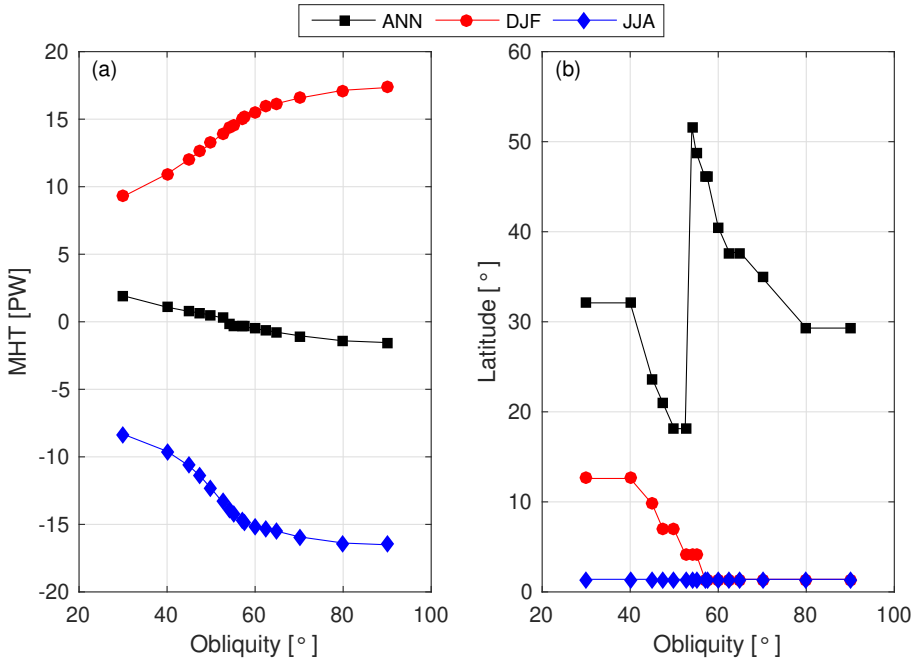

Figure 4.15: (a) Maximum value of MHT for each obliquity, (b) position of the maximum, in winter (DJF, red circles), summer (JJA, blue diamonds) and annual mean (black squares). Positive (negative) values indicate northward (southward) transport.

4.5 Atmospheric water vapor

Our Earth-like aquaplanets simulations have a blackbody equilibrium temperature ($T_{\rm eq}$) of 274 K. However, the annual mean global surface temperature ($T_{\rm glob}$) varies between 296 K and 305 K (Fig. 4.4) for changing obliquity. This rise of 22 K to 30 K from T_{eq} is a result of the atmosphere and its greenhouse effect causing $T_{\rm glob}$ to be warmer than T_{eq} in all our experiments.

$T_{\rm glob}$ increases because of atmospheric water vapor content, the main cause responsible for the greenhouse effect in these aquaplanets. The global mean precipitable water content in the atmosphere (PWV) increases almost twofold from $\delta = 30°$ to $\delta = 90°$, following the Clausius-Clapeyron relation (Fig. 4.16).

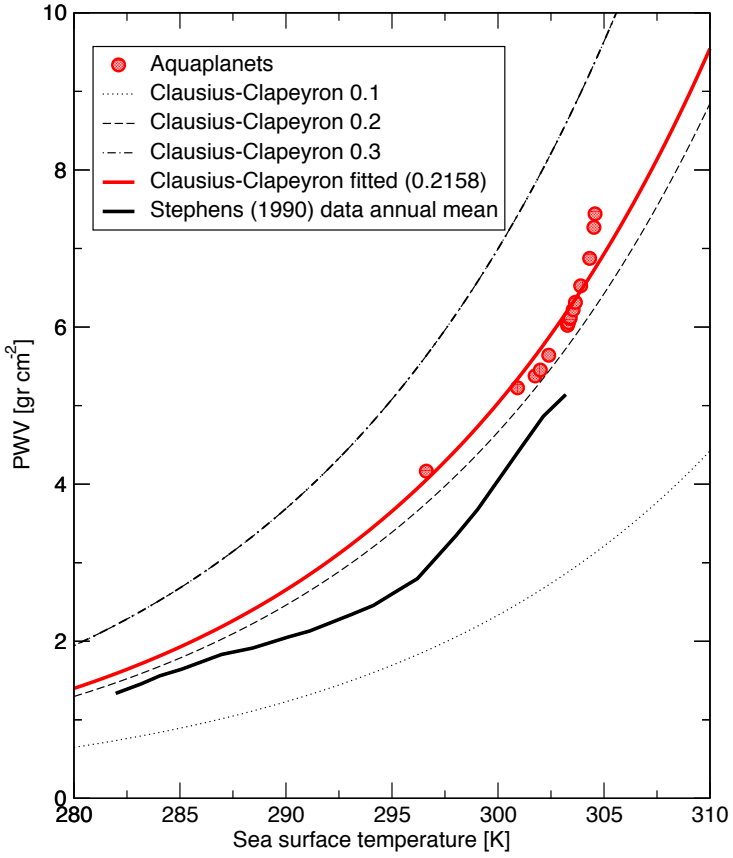

Figure 4.16: Examples of the Clausius-Clapeyron equation as in Stephens (1990) for $r/(1+\lambda)$ values between 0.1 and 0.3 (black lines). Red dots are aquaplanets values in the global and annual mean and red line indicates fit for $r/(1+\lambda) = 0.21$. The thick solid line corresponds to the measurements given as a function of SST by Stephens (1990) for Earth.

We applied the same algorithm used by Stephens (1990) to evaluate PWV as a function of SST. The best fit for our aquaplanets is obtained for $r/(1+\lambda) = 0.21$ (Fig. 4.16). Although the behavior is somewhat steeper at the highest temperatures ($80° \leq \delta \leq 90°$). We found for the aquaplanets a slightly higher value than the measurements given for Earth by Stephens (1990), but well within the limits of the parameters they proposed.

We can obtain PWV using Stephens (1990) equation:

$$PWV = 10.82 \left(\frac{r}{1+\lambda} \right) \mathrm{e}^{a(\mathrm{SST}-288)}, \tag{4.2}$$

where PWV is the precipitable water content in $\mathrm{gr\,cm^{-2}}$ and SST is sea surface temperature in K, with values above 288 K and $a \approx 0.064\,K^{-1}$. Using $r/(1+\lambda) = 0.21$ for aquaplanets at high obliquity.

Figure 4.17 shows the distribution of PWV and global atmospheric circulation for aquaplanets at different obliquities. When $\delta = 30°, 45°$ (see Figure 4.17a, 4.17b), water vapor is concentrated in the equatorial region due to the influence of the trade winds that converge in this area. The polar region has the lowest PWV amount in the aquaplanet with $\delta = 30°$ while in the aquaplanet with $\delta = 45°$, PWV has a homogeneous distribution throughout the planet due to a higher activity of the atmospheric circulation.

At high obliquities, the atmospheric circulation exhibits the divergence of winds in the equatorial region, the location of the easterly jet stream. The polar regions has highest amount of PWV in the atmosphere (see figure 4.17c), reaching a maximum PWV amount in the region at $\delta = 90°$ (see figure 4.17d).

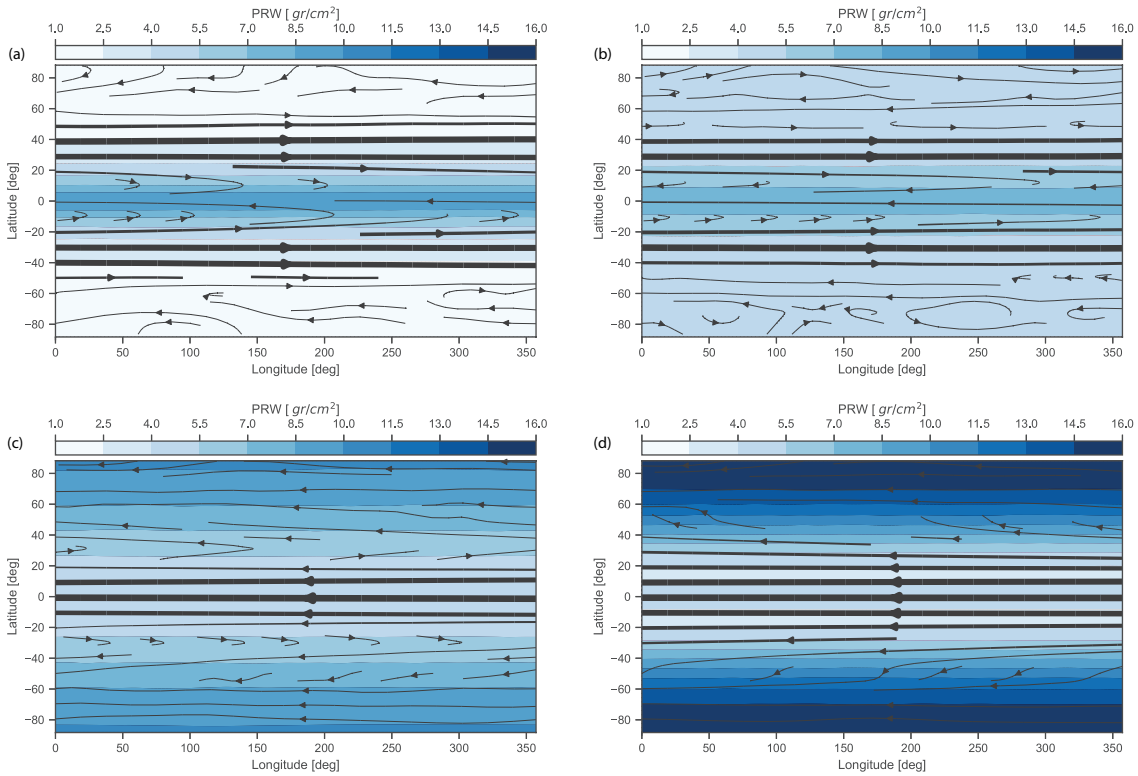

Figure 4.17: Zonal distribution of precipitable water vapor content and atmospheric circulation in JJA for aquaplanets at (a) $\delta = 30°$, (b) $\delta = 45°$, (c) $\delta = 60°$, (d) $\delta = 90°$. Precipitable water content in gr/cm^2 is presented in blue colors and the vertical mean of wind shown as black streamlines, the streamline wide is proportional to the wind magnitude.

4.5.1 Habitability

In this thesis, we evaluate planetary habitability depending on atmospheric water vapor. For this reason, we use the wet bulb temperature as an atmospheric index of habitability as was previously done by Sherwood and Huber (2010) in a future scenario of Earth with high global warming.

Atmospheric circulation plays a crucial role in distributing water vapor globally. In aqua-planets at high obliquity, the changes in winds regime cause more water vapor reaching polar regions (Fig 4.17), becoming wetter and warmer due to low-level clouds (Fig. 4.3). As evaporation becomes balanced with precipitation, a higher amount of water vapor remains in the atmosphere increasing the global greenhouse effect (Schneider et al., 2010).
High temperatures limit the development of complex life, especially in Earth-like atmospheres, with a high level of humidity.
We use the wet bulb temperature (T_w; Stull, 2011) which relates relative humidity (%) and air temperature (°C), as an atmospheric indicator for evaluating the latitudinal extent of habitability.
We define the habitable range as $0° \leq T_w \leq 35°$; because complex life such as mammals cannot survive above this temperature (Sherwood and Huber, 2010).
Figure 4.18 shows the habitability range defined by the wet bulb temperature. Hyperthermia (death by heat shock) is produced when air temperatures increase above $40°C$ with relative humidity values lower than 70%. As an example, on July 10, 1913, the air temperature of the Death Valley, USA reached $56.7°C$, with this temperature, a mammal could suffer hyperthermia with 20% of relative humidity.

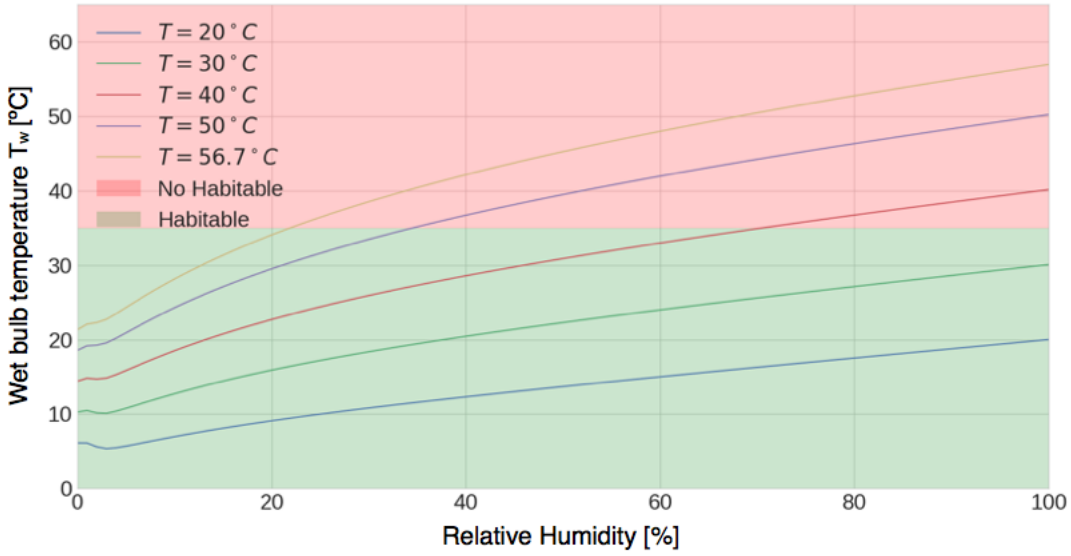

Figure 4.18: Examples of wet bulb temperature depending on air temperature (^oC) and relative humidity (%). The blue line indicates an air temperature of $20°C$; the green line indicates $30°C$, red line corresponds to $40°C$, the purple line shows $50°C$. The yellow line shows $56.7°C$ the highest temperature reached at Death Valley (USA) on July 10, 1913. Green and red area indicates the habitable and non-habitable ranges respectively, using the wet bulb temperature

Fig. 4.19 shows the percentage of months in which each aquaplanet falls within this habitability range. We have compared with Earth, but taking into account that cold temperatures constrain habitability.
Obliquities below $\delta = 54°$ are 100% habitable. Above $\delta = 70°$, year-long habitability is only possible in the region between latitudes $\pm 40°$, poleward of 40° latitude where humidity increases reducing habitability to half of the year.

Fig. 4.19 also shows that aquaplanets with obliquities above 30° have a higher latitudinal distribution of habitability than our planet.
We perform an Earth simulation with $\varepsilon = 0$, to compare the latitudinal extent of habitability. On Earth, only the latitudes between ±40° are 100% habitable under T_w habitability range, habitability decreases poleward as air temperature decreases, with $T_w < 0$. In the Northern hemisphere continents increase T_w maintaining this region half of the year habitable.

The analysis for habitability here presented corresponds to experiments that are ice-free for all months. In the case of either seasonal ice or snowball-earth conditions, this would alter the efficiency of latitudinal energy transport and could, therefore, lead to climatic instability (e.g., Kilic et al., 2017).

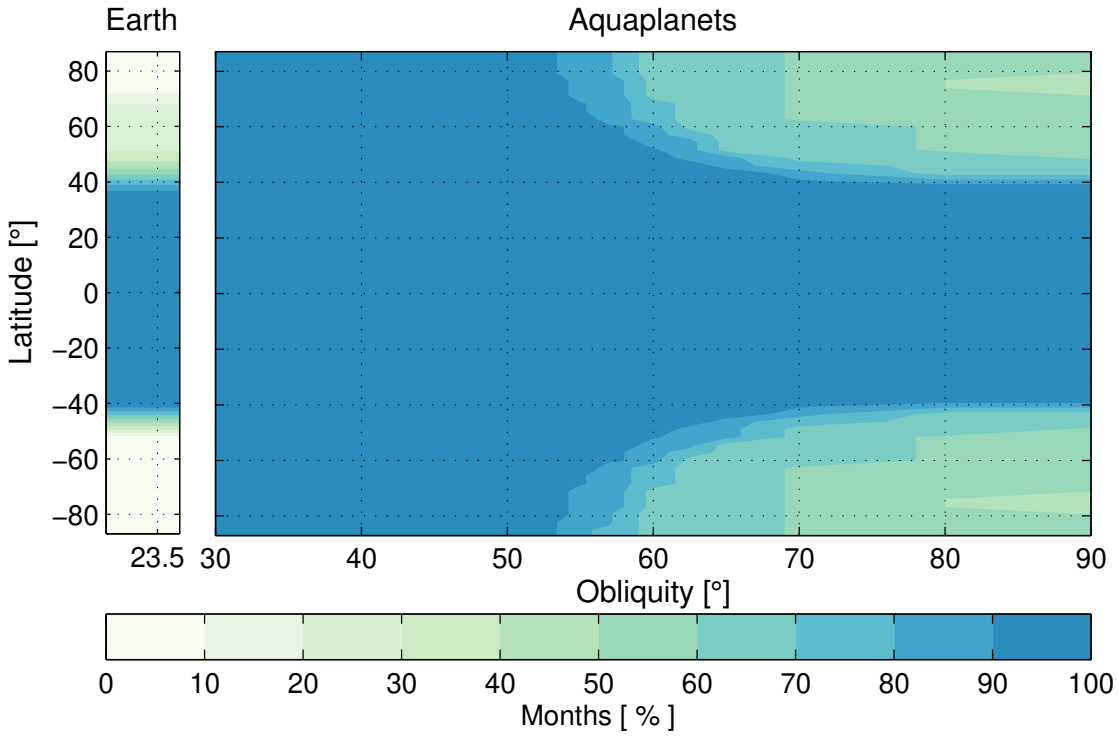

Figure 4.19: Latitudinal distribution of the monthly percentage of zonal mean habitability of each aquaplanet with all seasons ice-free conditions. Habitability is defined by a T_w temperature range of $0°C \leq T_w \leq 35°C$.

Chapter 5

Conclusions and future work

This thesis presented 16 aquaplanet experiments performed by varying its obliquity from 30° to 90° with finer sampling around 55°. Although the total amount of solar radiation that reaches the top of the atmosphere is the same for all experiments, changing obliquity has several effects.

Increasing obliquity produces a progressive change in the latitudinal insolation distribution from low to high obliquities. In the annual mean the insolation is the same at the equator and poles at $\delta = 54°$, acting as a pivot that divides the insolation distribution into two ranges: higher insolation at equator ($30° \leq \delta < 54°$), and higher insolation at the poles ($54° < \delta \leq 90°$). High obliquity increases seasonality. Both winter and summer become extreme as a larger proportion of the hemisphere stay in darkness in winter, and insolation increases its values up to 700 $\mathrm{W\,m^{-2}}$ in the summer hemisphere.

The atmospheric composition of the Earth-like aquaplanets determines the amount of radiation absorbed by its surface. A fraction of this radiation is reflected into space, while another fraction is absorbed by the atmosphere, depending on cloud cover (CC). The radiation absorbed by the surface reaches its maximum value at the aquaplanet with $\delta = 90°$, while CC and the reflected radiation present its minimum values. Nonetheless, solar radiation absorbed by the atmosphere stays constant in all our experiments. In terms of the large-scale atmospheric circulation, that redistributes the differential solar energy input, 54° is confirmed as the obliquity where a transition occurs, and the complete evolution of the two regimes is analyzed. For obliquities below 54°, when the equator receives more insolation than the poles, the large-scale circulation follows the known Earth's dynamics.
The latitudinal temperature gradient determines tropospheric westerly jet streams together with the Hadley and Ferrel cells and maximum precipitation in the tropics (the ITCZ), and the MHT is from low to high latitudes. As the latitudinal temperature gradients in the annual mean decrease close to obliquities of 54°, the circulation is less vigorous, with weaker overturning cells and jet streams and hence minimum MHT. However, because there are still significant seasonal variations, the circulation does not shut down as one could expect. For obliquities above 54°, the latitudinal temperature gradient reverses, and this has several important impacts. Easterly winds appear in the tropical troposphere at 200 hPa due to the reversed horizontal temperature gradient, especially in the summer hemisphere (also found

in Linsenmeier et al. (2015)). This wind differs from Earth, where Easterly winds appear in the stratosphere due to the increment of temperature by the ozone layer.

Figure 5.1 give an artist representation of the large scale atmospheric circulation on aquaplanets at obliquity $\delta = 45°$ and $\delta = 60°$. The left figure shows an aquaplanet with $\delta = 45°$ with high temperatures at the equatorial region. This latitudinal distribution of temperatures determines the wind regimes both in surface and in high levels, influencing the development of an easterly zonal wind around the equator.
Wind regime, presented here as the vertical mean of wind as figure 4.17, follows the same direction as Earth's wind in the aquaplanet with $\delta = 45°$, with easterly winds in tropical regions and westerlies at extratropical regions, but the wind regime changes at $\delta = 60°$ with a predominance of easterly winds which moves towards the poles in both hemispheres.
Hadley cells predominate over Ferrell and Polar cells, which disappear at this obliquity. Clouds cover most of the aquaplanet, and precipitations concentrate in the equatorial region. The right figure shows an aquaplanet with $\delta = 60°$ with high temperatures at the polar region. This latitudinal distribution of temperatures allows the easterly zonal wind increases its magnitude around the equator. Hadley cells become the predominant planetary cell.
Clouds cover the winter hemisphere in the aquaplanet. Precipitations maximum value remains in the equatorial region.

The regulating effect of the ocean is not an artifact of our modeling setup (slab ocean) but was also found in experiments with a fully dynamical ocean coupled to the atmosphere (Ferreira et al., 2014). As in their experiment, the ocean in our simulations acts as a reservoir releasing the stored heat into the atmosphere through convection, highlighting the importance of a liquid ocean in regulating the climate of a planet. We observe this effect in the global mean temperature that changes only 9 K as the obliquities increases from 30° to 90°.

Cloud cover diminishes as obliquity increases, affecting the amount of shortwave radiation absorbed by the surface. At high obliquity, the summer hemisphere present clear-sky conditions which allow increasing the radiation absorbed by the surface, meaning higher evaporation and an increment in the water vapor content in the atmosphere. As described in Schneider et al. (2010), warm climates simulations present a balance between evaporation and precipitation, due to the amount of solar radiation absorbed by the surface and latent heat flux released, which raises the concentration of water vapor in the atmosphere.

As was indicated by Sherwood and Huber (2010), atmospheric water vapor content determines habitability regions in our planet as high temperature and humidity conditions produce hyperthermia. We present the wet bulb temperature as an atmospheric index of habitability to determine the amount of time and location where aquaplanets with warm climate can be habitable. Habitability maps show that aquaplanets at high obliquity are more habitable than Earth under the same orbital conditions even when one of the hemispheres is in total darkness. Aquaplanets keep this completely latitudinal habitability during the year for obliquities under 54°. Above this value, habitability decreases toward the poles with half of the year habitable. These high obliquity aquaplanets maintain their 100% habitability between ±40° Latitude. Comparing with Earth, this is the region where our planet is completely habitable, and continents help to increase habitability toward the colder regions.

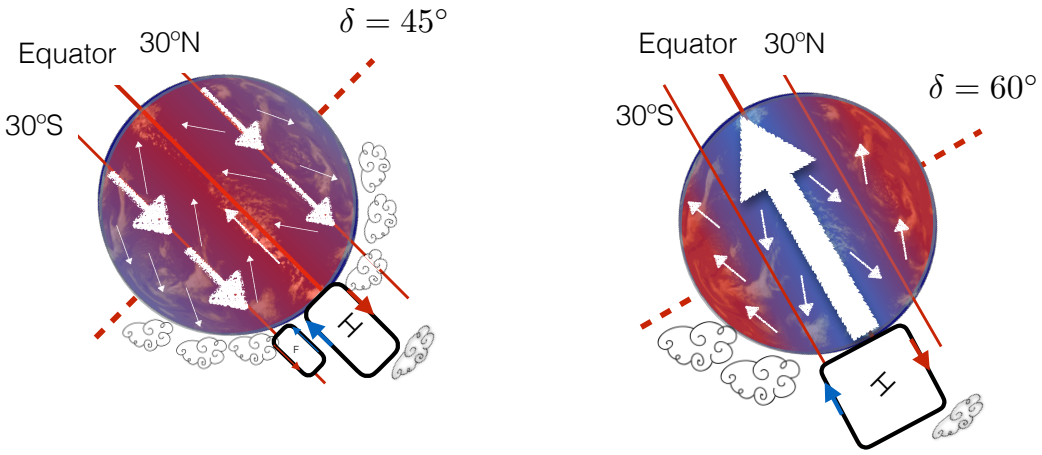

Figure 5.1: The schemes show the atmospheric circulation in aquaplanets with obliquities 45° and 60° in JJA mean. The dotted red line indicates the planet's rotation axis and the solid red lines indicate the latitudes 30°N, 30°S, and the Equator. The reddish tones that cover the planet present the regions of higher temperature, while the bluish tone presents the regions of lower temperature on the planet. White arrows indicate the wind regime as the vertical mean of wind, where the size of the arrow indicates the magnitude. Drawings of clouds indicate the regions where clouds predominated. Squares represent Hadley and Ferrel cells with arrows that indicate the air raising (red) and air descending (blue).

This thesis presented the characterization of the atmospheric variables that maintain a globally warm climate, ensuring the existence of liquid water on the surface of Earth-like aquaplanets with high obliquity, proving that these planets remain habitable due to atmospheric conditions.
This characterization raises many questions regarding the atmospheric dynamics of these planets. Although all these aquaplanets were modeled using terrestrial analogs, it was demonstrated that the atmospheric characteristics are far from what is observed on Earth, indicating how necessary is to study each of the variables presented here in greater detail.

As indicated, the total meridional heat transport is essential to maintain a warm climate ensuring habitability.
Although the methodology used for the calculation of the total meridional heat transport could give evidence of the existence of oceans and surface contrast a more detailed study of the mechanisms that affect the heat transport is needed as indicated by Donohoe et al. (2014). By using the decomposition of the total meridional heat transport such as Peixoto and Oort (1992), the perturbations related to the meridional circulation and the effect of the transient and stationary eddies are considered, affecting the energy distribution of the atmosphere. According to Lindzen and Hou (1988), the meridional circulation is influenced by the latitudinal displacement of the thermal gradient, which in this case is caused by the obliquity 52.5° which varies the region where the highest insolation occurs, affecting the development of the atmospheric meridional circulation.

The development of the easterly jet is one of the most interesting effects in high obliquity climate studies Linsenmeier et al. (2015), Ferreira et al. (2014). Unlike previous studies, limited by the number of simulations, this work presented the initial development of an

easterly jet stream at obliquity of 45° suggesting super-rotation and determining the presence of other sources, outside the thermal gradient, that can determine the position and extension of this zonal jet.

Concerning the simulations, this thesis was developed using a GCM with a 50 m slab ocean, the standard configuration for ocean depth in these models (Donohoe et al., 2014), which provides a reasonably accurate representation of previous works. However, as the aquaplanet simulation with $\delta = 23.5°$ converges into a snowball state after 40 years of simulation, further simulations are needed with different initial conditions of SST distribution. Moreover, a full atmospheric-ocean coupled model is necessary to attribute the snowball state to the lack of ocean heat transport in our slab-ocean GCM.
As indicated by Ferreira et al. (2014), the use of full coupled models are required to carry out habitability studies since the dynamic effect of the ocean must be included as oceanic circulation is also affected by obliquity variation.

While the existence of oceans in extrasolar planets could be measured through observational methods, (Cowan et al., 2009) the same does not happen with obliquity, although attempts to achieve it are currently under development (Seager and Deming, 2010, Kawahara, 2016).

Appendix A

Namelist parameters

The simulations use the following values in each namelist:

```
:::::::::::::::
ice_namelist
:::::::::::::::
&ICEPAR
NICE = 1
NFLUKO = 1
/END
:::::::::::::::
```

```
:::::::::::::::
land_namelist
:::::::::::::::
&LANDPAR
NBIOME = 0
ALBLAND=0.06
DZ0LAND=0.0002
/END
:::::::::::::::
```

```
:::::::::::::::
ocean_namelist
:::::::::::::::
&OCEANPAR
DLAYER = 50
NOCEAN = 1
NFLUKO = 1
/END
:::::::::::::::
```

```
:::::::::::::::
sea_namelist
:::::::::::::::
&seapar
ALBSEA = 0.06
/end
:::::::::::::::
```

```
:::::::::::::::
puma_namelist
:::::::::::::::
&INP
MARS     =0
NOUTPUT =1
NGUI     =0
N_START_YEAR=      1
N_DAYS_PER_YEAR=    360
N_RUN_YEARS=      50
N_RUN_MONTHS=      0
N_RUN_DAYS=      0
KICK     =      1
MPSTEP   =     20
NDIAG    =      0
NQSPEC   =      1
NWPD     =      1
NPRINT   =      0
/END
&PLANET
NFIXORB=1
ECCEN = 0
OBLIQ=23.5
YPLANET = "AQUA - OB23.5"
/END
&MISCPAR
/END
&FLUXPAR
/END
&RADPAR
NDCYCLE =      0
CO2      =   360.0000
DAWN     =     0.0000
GSOL0    =  1365.0000
/END
&RAINPAR
/END
&SURFPAR
/END
```

Figure A.1: Values defined for each namelist used in the experiments. The obliquity and the experiment name changes. Turning on the parameter NFLUKO allows the interaction between ice or ocean with the atmosphere.

Bibliography

Abbot, C.G., 1917. The sun and the weather. The Scientific Monthly 5, 400–410.

Batalha, N.M., Rowe, J.F., Bryson, S.T., Barclay, T., Burke, C.J., Caldwell, D.A., Christiansen, J.L., Mullally, F., Thompson, S.E., Brown, T.M., et al., 2013. Planetary candidates observed by kepler. iii. analysis of the first 16 months of data. The Astrophysical Journal Supplement Series 204, 24. doi:10.1088/0067-0049/204/2/24.

Berger, A., 1988. Milankovitch theory and climate. Reviews of geophysics 26, 624–657. doi:10.1029/RG026i004p00624.

Berger, A., 2012. A brief history of the astronomical theories of paleoclimates, in: Climate Change. Springer, pp. 107–129. doi:10.1007/978-3-7091-0973-1_8.

Bills, B.G., 1990. The rigid body obliquity history of Mars. Journal of Geophysical Research 95, 14137. doi:10.1029/JB095iB09p14137.

Borucki, W., Koch, D., Batalha, N., Caldwell, D., Christensen-Dalsgaard, J., Cochran, W.D., Dunham, E., Gautier, T.N., Geary, J., Gilliland, R., et al., 2008. Kepler: search for earth-size planets in the habitable zone. Proceedings of the International Astronomical Union 4, 289–299. doi:10.1017/S1743921308026513.

Borucki, W.J., Koch, D.G., Basri, G., Batalha, N., Brown, T.M., Bryson, S.T., Caldwell, D., Christensen-Dalsgaard, J., Cochran, W.D., DeVore, E., et al., 2011. Characteristics of planetary candidates observed by kepler. ii. analysis of the first four months of data. The Astrophysical Journal 736, 19. doi:10.1088/0004-637X/736/1/19.

Catling, D.C., 2013. Astrobiology: a very short introduction. OUP Oxford. doi:10.1002/gj.2690.

Cowan, N.B., Agol, E., Meadows, V.S., Robinson, T., Livengood, T.A., Deming, D., Lisse, C.M., A'Hearn, M.F., Wellnitz, D.D., Seager, S., et al., 2009. Alien maps of an ocean-bearing world. The Astrophysical Journal 700, 915. doi:10.1088/0004-637X/700/2/915.

Cowan, N.B., Voigt, A., Abbot, D.S., 2012. Thermal phases of earth-like planets: Estimating thermal inertia from eccentricity, obliquity, and diurnal forcing. The Astrophysical Journal 757, 80. doi:10.1088/0004-637X/757/1/80.

Crucifix, M., Loutre, M.F., Berger, A., 2006. The climate response to the astronomical

forcing. Space Science Reviews 125, 213–226.

Dahms, E., Lunkeit, F., Fraedrich, K., 2012. Low-frequency climate variability of an aquaplanet. Theoretical and Applied Climatology 121, 7932–. doi:10.1007/s00704-014-1226-8.

De Vera, J.P., Seckbach, J., et al., 2013. Habitability of other planets and satellites. Springer.

Dobrovolskis, A.R., Harris, A.W., 1983. The obliquity of Pluto. Icarus 55, 231–235. doi:10.1016/0019-1035(83)90077-5.

Donohoe, A., Battisti, D.S., 2012. What Determines Meridional Heat Transport in Climate Models? Journal of Climate 25, 3832–3850. doi:10.1175/JCLI-D-11-00257.1.

Donohoe, A., Frierson, D.M.W., Battisti, D.S., 2014. The effect of ocean mixed layer depth on climate in slab ocean aquaplanet experiments. Climate dynamics 43, 1041–1055. doi:10.1007/s00382-013-1843-4.

Dressing, C.D., Spiegel, D.S., Scharf, C.A., Menou, K., Raymond, S.N., 2010. Habitable climates: the influence of eccentricity. The Astrophysical Journal 721, 1295. doi:10.1088/0004-637X/721/2/1295.

Enderton, D., Marshall, J., 2009. Explorations of atmosphere–ocean–ice climates on an aquaplanet and their meridional energy transports. Journal of the Atmospheric Sciences 66, 1593–1611. doi:10.1175/2008JAS2680.1.

Ferreira, D., Marshall, J., O'Gorman, P.A., Seager, S., 2014. Climate at high-obliquity, in: Icarus, pp. 236–248. doi:10.1016/j.icarus.2014.09.015.

Fraedrich, K., Jansen, H., Kirk, E., Luksch, U., Lunkeit, F., 2005. The Planet Simulator: Towards a user friendly model. Meteorologische Zeitschrift 14, 299–304. doi:10.1127/0941-2948/2005/0043.

Hadley, G., et al., 1735. Vi. concerning the cause of the general trade-winds. Philosophical Transactions 39, 58–62. doi:10.1098/rstl.1735.0014.

Hart, M.H., 1978. The evolution of the atmosphere of the earth. Icarus 33, 23–39. doi:10.1016/0019-1035(78)90021-0.

Held, I.M., Hou, A.Y., 1980. Nonlinear Axially Symmetric Circulations in a Nearly Inviscid Atmosphere. Journal of the Atmospheric Sciences 37, 515–533. doi:10.1175/1520-0469(1980)037$<$0515:NASCIA$>$2.0.CO;2.

Holton, J.R., Hakim, G.J., 2012. An introduction to dynamic meteorology. volume 88. Academic press.

Imbrie, J., Berger, A., Boyle, E.A., Clemens, S.C., Duffy, A., Howard, W.R., Kukla, G., Kutzbach, J., Martinson, D.G., McIntyre, A., Mix, A.C., Molfino, B., Morley, J.J., Peterson, L.C., Pisias, N.G., Prell, W.L., Raymo, M.E., Shackleton, N.J., Toggweiler, J.R.,

1993. On the structure and origin of major glaciation cycles 2. The 100,000-year cycle. Paleoceanography 8, 699–735. doi:10.1029/93PA02751.

Ingersoll, A., 2013. Planetary climates. Princeton University Press.

Kallberg, P., Simmons, A., Uppala, S., Fuentes, M., 2004. The era-40 archive, era-40 project report series no. 17. European Center for Medium-Range Weather Forecasts, Reading, UK. http://www. ecmwf. int/publications/library/do/references/list/192 .

Kasting, J.F., 1988. Runaway and moist greenhouse atmospheres and the evolution of earth and venus. Icarus 74, 472–494. doi:10.1016/0019-1035(88)90116-9.

Kawahara, H., 2016. Frequency modulation of directly imaged exoplanets: Geometric effect as a probe of planetary obliquity. The Astrophysical Journal 822, 112. doi:10.3847/0004-637X/822/2/112.

Kiehl, J.T., Trenberth, K.E., 1997. Earth's annual global mean energy budget. Bulletin of the American Meteorological Society 78, 197–208. doi:10.1175/1520-0477(1997)078<0197:EAGMEB>2.0.CO;2.

Kilic, C., Raible, C., Stocker, T., 2017. Multiple climate states of habitable exoplanets: The role of obliquity and irradiance. The Astrophysical Journal 844, 13pp. doi:10.3847/1538-4357/aa7a03.

Kopparapu, R.K., Ramirez, R., Kasting, J.F., Eymet, V., Robinson, T.D., Mahadevan, S., Terrien, R.C., Domagal-Goldman, S., Meadows, V., Deshpande, R., 2013. Habitable zones around main-sequence stars: new estimates. The Astrophysical Journal 765, 131. doi:10.1088/0004-637X/765/2/131.

Kuo, H.L., 1956. Forced anf free meridional circulations in the atmosphere. Journal of Meteorology 13, 561–568. doi:10.1175/1520-0469(1956)013$<$0561:FAFMCI$>$2.0.CO;2.

Lammer, H., Selsis, F., Chassefière, E., Breuer, D., Grießmeier, J.M., Kulikov, Y.N., Erkaev, N.V., Khodachenko, M.L., Biernat, H.K., Leblanc, F., et al., 2010. Geophysical and atmospheric evolution of habitable planets. Astrobiology 10, 45–68. doi:10.1089/ast.2009.0368.

Laskar, J., Joutel, F., Robutel, P., 1993. Stabilization of the Earth's obliquity by the Moon. Nature 361, 615–617. doi:10.1038/361615a0.

Laskar, J., Robutel, P., 1993. The chaotic obliquity of the planets. Nature 361, 608–612. doi:10.1038/361608a0.

Lindzen, R.S., 1994. Climate dynamics and global change. Annual Review of Fluid Mechanics 26, 353–378. doi:10.1146/annurev.fl.26.010194.002033.

Lindzen, R.S., Hou, A.V., 1988. Hadley circulations for zonally averaged heating centered off the equator. Journal of the Atmospheric Sciences 45, 2416–2427. doi:10.1175/1520-0469(1988)045<2416:HCFZAH>2.0.CO;2.

Linsenmeier, M., Pascale, S., Lucarini, V., 2015. Climate of Earth-like planets with high obliquity and eccentric orbits: Implications for habitability conditions. Planetary and Space Science 105, 43–59. doi:10.1016/j.pss.2014.11.003, arXiv:arXiv:1401.5323v4.

Lorenz, E.N., 1967. The nature and theory of the general circulation of the atmosphere. volume 218. World Meteorological Organization Geneva.

Lowell, P., 1909. The evolution of worlds. Macmillan Company.

Lucarini, V., Pascale, S., Boschi, R., Kirk, E., Iro, N., 2013. Habitability and multistability in earth-like planets. Astronomische Nachrichten 334, 576–588. doi:10.1002/asna.201311903.

Marshall, J., Ferreira, D., Campin, J.M., Enderton, D., 2007. Mean climate and variability of the atmosphere and ocean on an aquaplanet. Journal of the Atmospheric Sciences 64, 4270–4286. doi:10.1175/2007JAS2226.1.

Marshall, J., Plumb, R.A., 2016. Atmosphere, ocean and climate dynamics: an introductory text. volume 21. Academic Press.

Mayor, M., Queloz, D., 1995. A jupiter-mass companion to a solar-type star. Nature 378, 355. doi:10.1038/378355a0.

Neale, R., 2000. A standard test for AGCMs including their physical parametrizations: I: The proposal. Atmospheric Science Letters 1, 101–107. doi:10.1006/asle.2000.0019.

Nielsen, A.C.W., Chen, T.C., 1993. Fundamentals of atmospheric energetics. Oxford University Press.

North, G.R., Erukhimova, T.L., 2009. Atmospheric Thermodynamics. Cambridge University Press, Cambridge. doi:10.1017/CBO9780511609695.

Nowajewski, P., Rojas, M., Rojo, P., Kimeswenger, S., 2018. Atmospheric dynamics and habitability range in earth-like aquaplanets obliquity simulations. Icarus doi:10.1016/j.icarus.2018.01.002.

Payne, R.E., 1972. Albedo of the Sea Surface. Journal of the Atmospheric Sciences 29, 959–970. doi:10.1175/1520-0469(1972)029$<$0959:AOTSS$>$2.0.CO;2.

Peixoto, J.P., Oort, A.H., 1992. Physics of climate. New York, NY (United States); American Institute of Physics.

Reiter, E., Greg, B., 2005. Jet Streams. Springer Netherlands. doi:10.1007/1-4020-3266-8_113".

Robock, A., 1980. The seasonal cycle of snow cover, sea ice and surface albedo. Monthly Weather Review 108, 267–285. doi:10.1175/1520-0493(1980)108<0267:TSCOSC>2.0.CO;2.

Sanchez-Lavega, A., 2011. An introduction to planetary atmospheres. CRC Press.

Satoh, M., 2013. Atmospheric circulation dynamics and general circulation models. Springer Science & Business Media.

Schneider, T., O'Gorman, P.A., Levine, X.J., 2010. Water vapor and the dynamics of climate changes. Reviews of Geophysics 48. doi:10.1029/2009RG000302.

Seager, S., 2013. Exoplanet Habitability. Science 33, 1231–1234. doi:10.1126/science.1232226.

Seager, S., Deming, D., 2010. Exoplanet atmospheres. Annual Review of Astronomy and Astrophysics 48, 631–672. doi:10.1146/annurev-astro-081309-130837.

Shapley, H., 1953. Climatic change: evidence, causes, and effects. Climatic Change: Evidence, Causes, and Effects .

Sherwood, S.C., Huber, M., 2010. An adaptability limit to climate change due to heat stress. Proceedings of the National Academy of Sciences 107, 9552–9555. doi:10.1073/pnas.0913352107.

Showman, A.P., Cho, J.Y., Menou, K., 2010. Atmospheric circulation of exoplanets. Exoplanets 526, 471–516.

Spiegel, D.S., Menou, K., Scharf, C.A., 2008. Habitable Climates. The Astrophysical Journal 681, 1609–1623. doi:10.1086/588089.

Stephens, G.L., 1990. On the Relationship between Water Vapor over the Oceans and Sea Surface Temperature. Journal of Climate 3, 634–645. doi:10.1175/1520-0442(1990)003$<$0634:OTRBWV$>$2.0.CO;2.

Stull, R., 2011. Wet-Bulb Temperature from Relative Humidity and Air Temperature. Journal of Applied Meteorology and Climatology 50, 2267–2269. doi:10.1175/JAMC-D-11-0143.1.

Sugiyama, M., Stone, P.H., Emanuel, K.A., 2005. The Role of Relative Humidity in Radiative–Convective Equilibrium. Journal of the Atmospheric Sciences 62, 2001–2011. doi:10.1175/JAS3434.1.

Touma, J., Wisdom, J., 1993. The chaotic obliquity of Mars. Science (New York, N.Y.) 259, 1294–1297. doi:10.1126/science.259.5099.1294.

Trenberth, K.E., Fasullo, J.T., Kiehl, J., 2009. Earth's global energy budget. Bulletin of the American Meteorological Society 90, 311–323. doi:10.1175/2008BAMS2634.1.

Vallis, G.K., 2017. Atmospheric and oceanic fluid dynamics. Cambridge University Press.

Vonder Haar, T.H., Oort, A.H., 1973. New estimate of annual poleward energy transport by northern hemisphere oceans. Journal of Physical Oceanography 3, 169–172. doi:10.1175/

1520-0485(1973)003<0169:NEOAPE>2.0.CO;2.

Wallace, J.M., Hobbs, P.V., 2006. Atmospheric science: an introductory survey. volume 92. Elsevier.

Ward, W.R., 1974. Climatic variations on Mars: 1. Astronomical theory of insolation. Journal of Geophysical Research 79, 3375–3386. doi:10.1029/JC079i024p03375.

Williams, D.M., Kasting, J.F., 1997. Habitable Planets with High Obliquities. Icarus 129, 254–267. doi:10.1006/icar.1997.5759.

Williams, D.M., Pollard, D., 2003. Extraordinary climates of Earth-like planets: three-dimensional climate simulations at extreme obliquity. International Journal of Astrobiology 2, 1–19. doi:10.1017/S1473550403001356.

Williamson, D.L., Blackburn, M., Nakajima, K., Ohfuchi, W., Takahashi, Y.O., Hayashi, Y.Y., Nakamura, H., Ishiwatari, M., McGregor, J.L., Borth, H., Wirth, V., Frank, H., Bechtold, P., Wedi, N.P., Tomita, H., Satoh, M., Zhao, M., Held, I.M., Suarez, M.J., Lee, M.I., Watanabe, M., Kimoto, M., Liu, Y., Wang, Z., Molod, A., Rajendran, K., Kitoh, A., Stratton, R., 2013. The Aqua-Planet Experiment (APE): Response to Changed Meridional SST Profile. Journal of the Meteorological Society of Japan. Ser. II 91A, 57–89. doi:10.2151/jmsj.2013-A03.